

One-loop contributions of charginos and neutralinos to W -pair production in e^+e^- collisions

Kaoru Hagiwara¹, Shinya Kanemura¹, Michael Klasen^{2*} and Yoshiaki Umeda^{3†}

¹*Theory Group, KEK, Tsukuba, Ibaraki 305-0801, Japan*

²*II Institut für Theoretische Physik, Universität Hamburg, D-22761 Hamburg, Germany*

³*Institut für Theoretische Physik E, RWTH Aachen, 52056 Aachen, Germany*

Abstract

We study the one-loop effects of charginos and neutralinos on the helicity amplitudes for $e^+e^- \rightarrow W^+W^-$ in the minimal supersymmetric standard model. The calculation is tested by using two methods. First, the sum rule for the form factors between $e^+e^- \rightarrow W^+W^-$ and the process where the external W^\pm bosons are replaced by the corresponding Goldstone bosons ω^\pm is employed to test the analytic expression and the accuracy of the numerical program. Second, the decoupling property in the large mass limit is used to test the overall normalization of the amplitudes. These two tests are most effectively carried out when the amplitudes are expanded in terms of the modified minimal subtraction ($\overline{\text{MS}}$) couplings of the standard model. The resulting perturbation expansion is valid at collider energies below and around the threshold of the light supersymmetric particles. We find that the corrections to the cross section of the longitudinally polarized W -pair production can be as large as -1.4% at the threshold of the light chargino-pair production for large scattering angles. We also study the effects of the CP -violating phase in the chargino and neutralino sectors on the helicity amplitudes. We find that the resulting CP -violating asymmetries can be at most 0.1% .

*Supported by DFG under contract Nr. KL 1266/1-3.

†Supported by BMBF, contract nr. 05 HT1PAA 4.

1 Introduction

W -boson-pair production has been the benchmark process of the CERN e^+e^- collider LEP2, and will continue being so at future linear e^+e^- collider experiments because of its large production rate and its possible sensitivity to the physics of electroweak symmetry breakdown. At linear colliders, precise measurements of the masses of the W boson, top quark, and possibly the Higgs boson will be achieved, and there is hope of detecting new physics signals through radiative corrections in the triple gauge boson ($WW\gamma$ and WWZ) vertices. In particular, if nature is described by the model with weak scale supersymmetry (SUSY), radiative corrections due to supersymmetric particles are expected.

In this paper, we show the one-loop effects of charginos and neutralinos on the helicity amplitudes of on-shell W -pair production in the minimal supersymmetric standard model (MSSM). A study of the contribution from squarks and sleptons has been reported in Ref. [1], and the range of one-loop corrections in the MSSM has been studied in the literature [2].

In Sec. 2, we review the essential aspects of the form-factor formalism and the helicity amplitudes for the process $e^+e^- \rightarrow W^+W^-$. A form-factor decomposition of helicity amplitudes [3, 4, 5] is useful to calculate the one-loop effects, and hence we present our result by extending the formalism of Ref. [6] such that the unphysical scalar polarization of the final-state W bosons can also be studied [7, 8]. These scalar polarization contributions and the process including the Nambu-Goldstone boson ($e^+e^- \rightarrow \omega^+ W^-$) are necessary to perform the test by using the Becchi-Rouet-Stora (BRS) sum rules [8].

In Sec. 3, the one-loop chargino and neutralino effects on the gauge couplings, the weak boson masses, and the form factors are presented in the modified minimal subtraction ($\overline{\text{MS}}$) scheme [9]. In Sec. 4, our one-loop calculation for the amplitude is tested by using the BRS sum rule and the decoupling property. First, the BRS sum rule for the form factors between $e^+e^- \rightarrow W^+W^-$ and $e^+e^- \rightarrow \omega^+ W^-$ is used to test the analytic expressions and the accuracy of the numerical program. This test is useful in the process $e^+e^- \rightarrow W^+W^-$ where the gauge theory cancellation among one-loop diagrams becomes severe at high energies. We confirm numerically that the form factors satisfy the BRS sum rule within the expected accuracy of the numerical program. Second, the decoupling property in the large mass limit is used to test the normalization of the amplitudes. By expanding the one-loop amplitudes in terms of the $\overline{\text{MS}}$ couplings of the SM, the decoupling of the SUSY particle effects is made manifest in the large mass limit. This test ensures the validity of the renormalization scheme and confirms the overall normalization factors such as the external wave-function contribution, which cannot be tested by the BRS sum rules. We find that the above two tests are most effectively carried out when the amplitudes are expanded in terms of the $\overline{\text{MS}}$ couplings of the standard model. The resulting perturbation expansion is valid at collider energies below and around the light SUSY particle thresholds.

In Sec. 5, we present a numerical study of the $e^+e^- \rightarrow W^+W^-$ helicity amplitudes. We also examine the effects of the CP -violating phases of the chargino and neutralino sector. In Sec. 6 we

present our conclusion.

In Appendix A, we summarize our notation for the mass terms and the interactions of the chargino and neutralino sector of the MSSM. The formulas for the one-loop contributions to the two-point functions and the vertex functions are listed in Appendix B.

2 The helicity amplitudes

2.1 $e^+e^- \rightarrow W^+W^-$

We consider the process

$$e^-(k, \tau) + e^+(\bar{k}, \bar{\tau}) \rightarrow W^-(p, \lambda) + W^+(\bar{p}, \bar{\lambda}), \quad (2.1)$$

where the incoming momenta of e^- and e^+ are k and \bar{k} as well as the outgoing momenta of W^- and W^+ are p and \bar{p} , respectively. The helicity of the incoming e^- (e^+) is given by $\frac{1}{2}\tau$ ($\frac{1}{2}\bar{\tau}$), and that of the outgoing W^- (W^+) is given by λ ($\bar{\lambda}$). In the limit of massless electrons, only the $\bar{\tau} = -\tau$ helicity amplitudes survive. They are written for each set of $\{\tau, \lambda, \bar{\lambda}\}$ as [6, 8]

$$\mathcal{M}_\tau^{\lambda\bar{\lambda}}(e^+e^- \rightarrow W^+W^-) = \sum_{i=1}^{16} F_{i,\tau}(s, t) j_\mu(k, \bar{k}, \tau) T_i^{\mu\alpha\beta} \epsilon_\alpha(p, \lambda)^* \epsilon_\beta(\bar{p}, \bar{\lambda})^*, \quad (2.2)$$

where all dynamical information is contained in the form factors $F_{i,\tau}(s, t)$ with $s = (k + \bar{k})^2 \equiv q^2$ and $t = (k - p)^2$. The other factors in Eq. (2.2) are of a purely kinematical nature; $\epsilon_\alpha(p, \lambda)^*$ and $\epsilon_\beta(\bar{p}, \bar{\lambda})^*$ are the polarization vectors for W^- and W^+ , respectively, and $j_\mu(k, \bar{k}, \tau)$ is the massless-electron current. The 16 independent basis tensors $T_i^{\mu\alpha\beta}$ are defined by Eqs. (2.6) in Ref. [8]. Processes with physically polarized W bosons ($\lambda, \bar{\lambda} = -, +$ or 0) are described by the first nine form factors ($i = 1$ to 9 for $\tau = \pm 1$).

The 18 physical helicity amplitudes are given in terms of the form factors $F_{1,\tau}$ to $F_{9,\tau}$ by ¹

$$M_\tau^{00} = -s \left[-\gamma^2 \beta (1 + \beta^2) F_{1,\tau} + 4\beta^3 \gamma^4 F_{2,\tau} + 2\beta \gamma^2 F_{3,\tau} - 2\gamma^2 \cos \theta F_{8,\tau} \right] \sin \theta, \quad (2.3a)$$

$$M_\tau^{\pm 0} = s \gamma \left[\beta (F_{3,\tau} - i F_{4,\tau} \pm \beta F_{5,\tau}) \pm i F_{6,\tau} \pm (\tau \mp 2 \cos \theta) F_{8,\tau} \mp 4\gamma^2 \beta \cos \theta F_{9,\tau} \right] \frac{(\tau \pm \cos \theta)}{\sqrt{2}}, \quad (2.3b)$$

$$M_\tau^{0\pm} = s \gamma \left[\beta (F_{3,\tau} + i F_{4,\tau} \mp \beta F_{5,\tau}) \pm i F_{6,\tau} \mp (\tau \pm 2 \cos \theta) F_{8,\tau} \pm 4\gamma^2 \beta \cos \theta F_{9,\tau} \right] \frac{(\tau \mp \cos \theta)}{\sqrt{2}}, \quad (2.3c)$$

$$M_\tau^{\pm\pm} = s \left[-\beta F_{1,\tau} \mp i F_{6,\tau} \mp 4i\beta^2 \gamma^2 F_{7,\tau} + \cos \theta F_{8,\tau} + 4\beta \gamma^2 \tau F_{9,\tau} \right] \sin \theta, \quad (2.3d)$$

$$M_\tau^{\pm\mp} = s (\mp F_{8,\tau} - 4\beta \gamma^2 F_{9,\tau}) (\tau \pm \cos \theta) \sin \theta, \quad (2.3e)$$

where the scattering angle θ is measured between the momentum vectors of the e^- and W^- ,

$$\beta = \sqrt{1 - m_W^2/E_W^2}, \quad \gamma = E_W/m_W, \quad E_W = \sqrt{s}/2, \quad (2.4)$$

in the center-of-mass frame of e^+e^- collision. The properties of $F_{i,\tau}(s, t)$ under the discrete transformations of the charge conjugation (C), the parity inversion (P), and the combined transformation CP are summarized in Table 1. There are six CP -violating form factors ($F_{4,\tau}$, $F_{6,\tau}$, and $F_{7,\tau}$).

¹In Ref. [1], there is a typo in the expression for $M^{0\pm}$. The corrected one is given in Eq. (2.3c) in this paper.

	F_1	F_2	F_3	F_4	F_5	F_6	F_7	F_8	F_9
C	+	+	+	−	−	+	+	+	−
P	+	+	+	+	−	−	−	+	−
CP	+	+	+	−	+	−	−	+	+

Table 1: The properties of the form factors $F_{i,\tau}(s, t)$ under the discrete transformations C , P , and CP . Only those that contribute to physical processes are listed.

The remaining 14 form factors ($i = 10$ to 16 for $\tau = \pm 1$) contribute to the amplitudes including unphysical polarizations of the W bosons ($\lambda, \bar{\lambda} = S$), where the polarization vectors are $\epsilon^\alpha(p, \lambda = S)^* = p^\alpha/m_W$ and $\epsilon^\beta(\bar{p}, \bar{\lambda} = S)^* = \bar{p}^\beta/m_W$.

2.2 $e^+e^- \rightarrow \omega^+W^-$

To test the $e^+e^- \rightarrow W^+W^-$ form factors by using the BRS sum rules, we also calculate the unphysical process

$$e^-(k, \tau) + e^+(\bar{k}, \bar{\tau}) \rightarrow W^-(p, \lambda) + \omega^+(\bar{p}), \quad (2.5)$$

where ω^+ is the Nambu-Goldstone boson associated with W^+ . Our phase convention for ω^+ is that of Ref. [7]. We decompose the helicity amplitudes as

$$\mathcal{M}_\tau^\lambda(e^+e^- \rightarrow \omega^+W^-) = i \sum_{i=1}^4 H_{i,\tau}(s, t) j_\mu(k, \bar{k}, \tau) S_i^{\mu\alpha} \epsilon_\alpha(p, \lambda)^*. \quad (2.6)$$

In Eq. (2.6), there are four independent basis tensors, $S_i^{\mu\alpha}$ ($i = 1-4$), corresponding to the four (three physical plus one scalar) polarizations of the W^- boson. The form factors are given by $H_{i,\tau}(s, t)$. The basis tensors $S_i^{\mu\alpha}$ are given in Eq. (2.9) of Ref [8].

3 One-loop chargino and neutralino contributions

In this section, we calculate the one-loop contributions of charginos and neutralinos to the form factors $F_{i,\tau}$ for $e^+e^- \rightarrow W^+W^-$ and $H_{i,\tau}$ for $e^+e^- \rightarrow \omega^+W^-$. The Lagrangian for the chargino and neutralino sector of the MSSM [10] is given in Appendix A, in order to fix our notation.

3.1 The renormalization scheme

We explain our renormalization scheme of the MSSM parameters, which is designed to make the BRS sum rules exact in the one-loop order. First, we take the physical W boson mass m_W as one of our input parameters as in Ref. [1]. The $\overline{\text{MS}}$ coupling constants $\hat{e}^2(\mu_R)$ and $\hat{g}^2(\mu_R) = \hat{e}^2(\mu_R)/\hat{s}^2(\mu_R)$ of the MSSM are used as the expansion parameters for perturbation calculation. They are obtained

from the $\overline{\text{MS}}$ couplings of the SM by using the matching conditions

$$\frac{16\pi^2}{\hat{e}^2(\mu_R)} = \frac{16\pi^2}{\hat{e}_{\text{SM}}^2(\mu_R)} - \left[\frac{4}{3} \log \frac{\mu_R^2}{m_{\tilde{\chi}_1^-}^2} + \frac{4}{3} \log \frac{\mu_R^2}{m_{\tilde{\chi}_2^-}^2} \right], \quad (3.1a)$$

$$\frac{16\pi^2}{\hat{g}^2(\mu_R)} = \frac{16\pi^2}{\hat{g}_{\text{SM}}^2(\mu_R)} - \left[\frac{2}{3} \{(D_L)_{11} + (D_R)_{11}\} \log \frac{\mu_R^2}{m_{\tilde{\chi}_1^-}^2} + \{(D_L)_{22} + (D_R)_{22}\} \log \frac{\mu_R^2}{m_{\tilde{\chi}_2^-}^2} \right], \quad (3.1b)$$

where all the additional particles in the MSSM (squarks, sleptons, and extra Higgs bosons) are assumed to be heavy. Only the chargino mass $m_{\tilde{\chi}_i^-}$ ($i = 1$ and 2) appears in the matching conditions, and the matrices $(D_\alpha)_{ij}$ that relate the weak eigenstates to the mass eigenstates are defined in Appendix B 3. The numerical results of this report are obtained for

$$m_W = 80.41 \text{ GeV}, \quad \hat{e}_{\text{SM}}^2(m_Z)/(4\pi) = 1/128.06, \quad \text{and} \quad \hat{s}_{\text{SM}}^2(m_Z) = 0.2313, \quad (3.2)$$

where the values of $\hat{e}_{\text{SM}}^2(m_Z)$ and $\hat{s}_{\text{SM}}^2(m_Z)$ are obtained for $m_t = 175 \text{ GeV}$. The remaining $\overline{\text{MS}}$ coupling constants of the SM are then calculated in the leading order by using Eqs. (3.5a) and (3.5b) in Ref. [1]. The above conditions ensure that physical observables at low energies remain the same when all the chargino and neutralino masses are large. In this paper, we do not consider contributions of sfermions, gluinos, or additional Higgs scalar bosons. These particles are assumed to be very heavy, and we work within the effective MSSM with light charginos and neutralinos. The three input parameters $\{m_W, \hat{e}^2(\mu_R), \hat{s}^2(\mu_R)\}$ are consistently employed in the evaluation of all loop integrals and form factors, as well as the chargino and neutralino mixing matrix elements. All the terms of the relevant diagrams are expanded in powers of the $\overline{\text{MS}}$ coupling \hat{g}^2 (or \hat{e}^2), and the terms up to $\mathcal{O}(\hat{g}^4)$ are taken into account.

The $\overline{\text{MS}}$ masses of the weak bosons are calculated in the one-loop level as

$$\hat{m}_W^2 = m_W^2 + \Pi_T^{WW}(m_W^2), \quad (3.3)$$

$$\hat{m}_Z^2 = \frac{\hat{m}_W^2}{\hat{c}^2} = \frac{1}{\hat{c}^2} \{m_W^2 + \Pi_T^{WW}(m_W^2)\}, \quad (3.4)$$

where $\Pi_T^{WW}(q^2)$ is the W boson two-point function in the $\overline{\text{MS}}$ scheme [11], whose chargino and neutralino contribution is given in Appendix B 3. The Z boson mass is then obtained as

$$m_Z^2 = \frac{m_W^2}{\hat{c}^2} + \frac{1}{\hat{c}^2} \Pi_T^{WW}(m_W^2) - \Pi_T^{ZZ} \left(\frac{m_W^2}{\hat{c}^2} \right) \equiv \frac{m_W^2}{\hat{c}^2} + \Delta. \quad (3.5)$$

The chargino and neutralino contributions to the two-point functions Π_T^{WW} and Π_T^{ZZ} are given in Appendix B 3, and the deviation from the tree-level expression is denoted by Δ . In order to preserve the BRS invariance of the one-loop amplitudes exact, the Z -boson propagator should be expanded and truncated as [8]

$$\frac{1}{s - m_Z^2} = \frac{1}{s - (m_W^2/\hat{c}^2)} \left\{ 1 + \frac{\Delta}{s - m_W^2/\hat{c}^2} \right\}. \quad (3.6)$$

3.2 One-loop form factors

At the one-loop level, the form factors $F_{i,\tau}(s, t)$, which have been introduced in Eq. (2.2), may be written as

$$F_{i,\tau} = F_{i,\tau}^{(0)} + F_{i,\tau}^{(1)}, \quad (3.7)$$

where $F_{i,\tau}^{(0)}$ and $F_{i,\tau}^{(1)}$ are the $\mathcal{O}(\hat{g}^2)$ and $\mathcal{O}(\hat{g}^4)$ contributions, respectively. We are interested in the $e^+e^- \rightarrow W^+W^-$ amplitudes for physically polarized W bosons ($\lambda, \bar{\lambda} = 0, \pm$). In order to test the form factors by using the BRS sum rules, we also have to consider the cases in which one or two external W bosons have scalar polarization; *i.e.*, λ and/or $\bar{\lambda} = S$. Since the BRS sum rules can test the form factors except for the overall factors such as the wave-function renormalization contribution, we find it convenient to divide the one-loop contribution $F_{i,\tau}^{(1)}$ into the following two parts: One is the contributions of the external W -boson wave-function renormalization ($F_{i,\tau}^{(1)\text{ext}}$), and the other is the rest ($F_{i,\tau}^{(1)\text{int}}$). Equation (3.7) is then rewritten as

$$F_{i,\tau} = F_{i,\tau}^{(0)} + F_{i,\tau}^{(1)\text{int}} + F_{i,\tau}^{(1)\text{ext}} \equiv \tilde{F}_{i,\tau} + F_{i,\tau}^{(1)\text{ext}}. \quad (3.8)$$

The explicit forms of $\tilde{F}_{i,\tau}$ and $F_{i,\tau}^{(1)\text{ext}}$ are given in Appendix B 1. Here, $\tilde{F}_{i,\tau}$ includes all the one-loop as well as tree-level contributions except for the external W -boson wave-function corrections. This part of the form factors, $\tilde{F}_{i,\tau}$, will be tested by the BRS sum rules in Sec. 4.1, while the overall normalization is verified by using the decoupling property of the chargino and neutralino contributions in the large chargino and neutralino mass limit in Sec. 5.2. For the BRS test we have to calculate all 32 form factors $\tilde{F}_{i,\tau}$ ($i = 1 - 16$) for each τ , while we have to calculate the $F_{i,\tau}^{(1)\text{ext}}$ only for the physical external W lines ($i = 1 - 9$). The one-loop level form factors $H_{i,\tau}$ for the process $e^+e^- \rightarrow \omega^+W^-$ are given in Appendix B 2.

4 Test of the loop calculation

The purpose of this paper is to evaluate quantitatively the one-loop contributions of charginos and neutralinos to the process $e^+e^- \rightarrow W^+W^-$. In order to ensure the correctness of our calculation, we examine in this section the BRS invariance of our one-loop amplitudes and the decoupling behavior of the SUSY effects in the large mass limit of charginos and neutralinos.

4.1 The BRS sum rules for the $e^+e^- \rightarrow W^+W^-$ form factors

The standard electroweak theory after gauge fixing is invariant under global BRS symmetry, so that the amplitudes, that include external massive gauge bosons are related to the amplitudes where some of those gauge bosons are replaced by their Nambu-Goldstone-boson counterparts. From the BRS invariance, the following relations between $e^+e^- \rightarrow W^+W^-$ and $e^+e^- \rightarrow \omega^+W^-$ amplitudes are obtained [8, 1]

$$\mathcal{M}(e^+e^- \rightarrow W_S^+ W_P^-) + iC_{\text{mod}}^{\text{BRS}} \mathcal{M}(e^+e^- \rightarrow \omega^+ W_P^-) = 0, \quad (4.1)$$

where W_P denotes the physical W -boson states ($\lambda = \pm 1, 0$) and W_S denotes its scalar polarization state ($\lambda = S$). At loop levels, the factor C_{mod}^{BRS} is not unity, and it is found to be [8]

$$C_{\text{mod}}^{BRS} = \frac{\hat{m}_W}{m_W}. \quad (4.2)$$

By inserting the expressions (2.2) and (2.6) into the BRS identity, we obtain the following six sum rules:

$$-2\gamma^2 \left\{ \tilde{F}_{3,\tau}(s, t) - i\tilde{F}_{4,\tau}(s, t) \right\} + 4\delta^2 \tilde{F}_{8,\tau}(s, t) + \tilde{F}_{13,\tau}(s, t) = C_{\text{mod}}^{BRS} H_{1,\tau}(s, t), \quad (4.3a)$$

$$-\tilde{F}_{1,\tau}(s, t) + 2\gamma^2 \tilde{F}_{2,\tau}(s, t) + \frac{1}{2}\tilde{F}_{3,\tau}(s, t) + \frac{i}{2}\tilde{F}_{4,\tau}(s, t) + \tilde{F}_{14,\tau}(s, t) = C_{\text{mod}}^{BRS} H_{2,\tau}(s, t), \quad (4.3b)$$

$$-\frac{1}{2}\tilde{F}_{5,\tau}(s, t) - \frac{i}{2}\tilde{F}_{6,\tau}(s, t) - \frac{\tau}{2}\tilde{F}_{8,\tau}(s, t) + 2\delta^2 \tilde{F}_{9,\tau}(s, t) + \tilde{F}_{15,\tau}(s, t) = C_{\text{mod}}^{BRS} H_{3,\tau}(s, t), \quad (4.3c)$$

where

$$\gamma^2 = \frac{s}{4m_W^2}, \quad \delta^2 = \frac{s + 2t - 2m_W^2}{4m_W^2}. \quad (4.4)$$

Among the 18 physical form factors ($\tilde{F}_{1,\tau}$ through $\tilde{F}_{9,\tau}$ for $\tau = \pm 1$), all but the two CP -violating form factors $\tilde{F}_{7,\tau}$ ($\tau = \pm$) appear in the sum rules. The form factors $\tilde{F}_{7,\tau}$ should be tested by other means. We find that the chargino and neutralino contributions to $\tilde{F}_{7,\tau}$ are zero at the one-loop order. The remaining 16 physical form factors are tested by the sum rules (4.3a)-(4.3c), where $\tilde{F}_{13,\tau}$ through $\tilde{F}_{15,\tau}$ are obtained from the $e^+e^- \rightarrow W^+W^-$ amplitude, and $H_{1,\tau}$ through $H_{3,\tau}$ from the $e^+e^- \rightarrow \omega^+W^-$ amplitude. This extra effort is worthwhile because the test is very powerful; each form factor has its own complicated dependence on s and t .

We apply the BRS sum rules also for testing the numerical program. For this purpose, we have formulated the BRS sum rules to hold exactly for the one-loop form factors. Both sides of the six BRS sum rules should then agree within the expected accuracy of the numerical computation. We have confirmed that all six sum rules (4.3a)-(4.3c) hold to better than 11-digit accuracy at e^+e^- collision energies \sqrt{s} at 200, 500, and 1000 GeV. In the evaluation of the scalar one-loop integral functions, we have partly used the Fortran FF package [12].

4.2 Decoupling limit

The one-loop effects of the SUSY particles should decouple from the low energy observable in the large mass limit. The theory should then become effectively the SM. In the $\overline{\text{MS}}$ scheme, perturbation expansion is performed by the $\overline{\text{MS}}$ couplings of the MSSM, so that it is nontrivial to see the above statement of the decoupling clearly. In order to show the decoupling openly, we use the $\overline{\text{MS}}$ couplings of the SM as the expansion parameter of the perturbation theory. This is clearly the most convenient scheme below the SUSY particle threshold. We adopt this scheme even above the threshold, because the difference from the results in the $\overline{\text{MS}}$ is found to be numerically very small [1] as long as the logarithms of the ratios s/m_{SUSY}^2 are not too large.

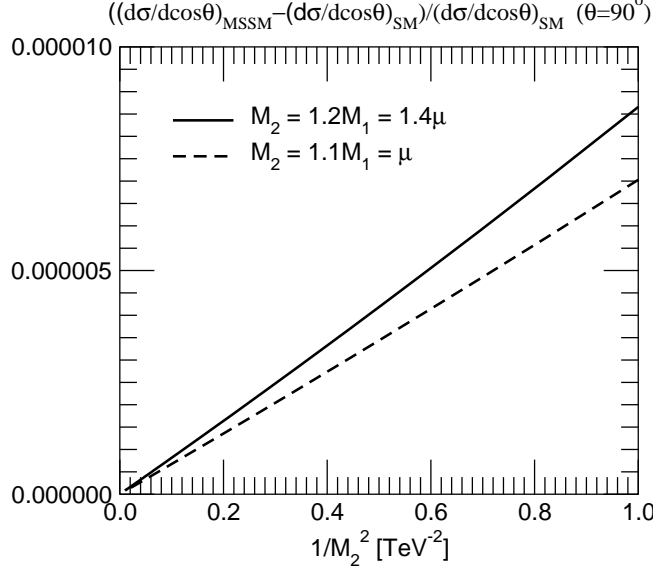


Figure 1: The test of decoupling of the chargino and neutralino contributions. The deviation of the helicity summed cross section from the SM value versus $1/M_2^2$ is shown at $\sqrt{s} = 200$ GeV and the scattering angle $\theta = 90^\circ$, where M_2 is the gaugino mass. The solid line is for $M_2 = 1.2M_1 = 1.4\mu$, and the dashed line is for $M_2 = 1.1M_1 = \mu$.

In order to obtain a perturbative expression in terms of the $\overline{\text{MS}}$ couplings of the SM, we insert the expansion (3.1):

$$\hat{e}^2(\mu_R) = \hat{e}_{\text{SM}}^2(\mu_R) \left\{ 1 + \frac{4}{3} \left[\log \frac{\mu_R^2}{m_{\tilde{\chi}_1^-}^2} + \log \frac{\mu_R^2}{m_{\tilde{\chi}_2^-}^2} \right] \frac{\hat{e}_{\text{SM}}^2(\mu_R)}{16\pi^2} \right\}, \quad (4.5a)$$

$$\hat{g}^2(\mu_R) = \hat{g}_{\text{SM}}^2(\mu_R) \left\{ 1 + \frac{2}{3} \left[\{(D_L)_{11} + (D_R)_{11}\} \log \frac{\mu_R^2}{m_{\tilde{\chi}_1^-}^2} + \{(D_L)_{22} + (D_R)_{22}\} \log \frac{\mu_R^2}{m_{\tilde{\chi}_2^-}^2} \right] \frac{\hat{g}_{\text{SM}}^2(\mu_R)}{16\pi^2} \right\}, \quad (4.5b)$$

in all the form factors, and we retain only terms up to $\mathcal{O}(\hat{g}_{\text{SM}}^4)$. Hereafter, we perform this procedure in all our calculations. As a result of the expansion by SM coupling, there is exactly no renormalization point dependence in our calculation.

In the large mass limit for charginos and neutralinos, the one-loop amplitudes behave as

$$\delta\mathcal{M}^{\text{Ino-loop}} \sim A + B \frac{s}{m_{\tilde{\chi}}^2} + \mathcal{O}\left(\frac{s^2}{m_{\tilde{\chi}}^4}\right). \quad (4.6)$$

In the original expression for the amplitudes in terms of the MSSM $\overline{\text{MS}}$ couplings, the constant term A remains nonzero because higher order terms of $\mathcal{O}(\hat{g}^6)$ do not cancel exactly. On the other hand, in our scheme in which such higher order terms are systematically eliminated in the analytic expressions, the term A in Eq. (4.6) is exactly zero, and the decoupling of the chargino and neutralino effects is made manifest. This property of the *exact decoupling* in our scheme can be used for an excellent test

	1	2	3	4	5	6	7
Parameter							
$\text{sgn}(\mu)$	+	−	+	−	+	+	+
$\tan\beta$	3	3	50	50	3	3	3
$m_{\tilde{\chi}_1^-}$ (GeV)	110	110	110	110	130	150	170

Table 2: The parameter sets for figures of showing $|\mu|$ dependence. Sets 1–4 are for Fig. 3(a), Fig. 4(a), and Fig. 6(a). Sets 5–7 are used in Fig. 5.

of the one-loop calculation including the overall normalization factors such as the W -boson wave-function renormalization constants that are not tested by the BRS sum rules. Figure 1 shows the chargino and neutralino contributions in the helicity summed differential cross section as a function of $1/M_2^2$ at $\sqrt{s} = 200\text{GeV}$ and the scattering angle $\theta = 90^\circ$, where M_2 is the gaugino mass. The solid line is for $M_2 = 1.2M_1 = 1.4\mu$, and the dashed line is for $M_2 = 1.1M_1 = \mu$. We can see that the helicity summed differential cross section in the MSSM becomes that of the SM in both cases at large mass of the gaugino.

5 Numerical evaluation of the chargino and neutralino effects on $e^+e^- \rightarrow W^+W^-$

Having tested the numerical program in the last section, we are ready to study the one-loop chargino and neutralino contribution to the $e^+e^- \rightarrow W^+W^-$ helicity amplitudes. We present here the results of the one-loop contributions to the helicity amplitudes as a function of the Higgs mixing parameter μ as well as of the e^+e^- collider energy \sqrt{s} .

In Secs. 5.1 to 5.3, we show the results for CP conserving cases. The free parameters in the chargino and neutralino sectors are then the μ parameter (and its sign), the ratio of the vacuum expectation value $\tan\beta$, and the soft SUSY breaking gaugino masses M_1 and M_2 for $U(1)$ and $SU(2)$, respectively. For simplicity, we assume the relation $M_1 = 5M_2\hat{s}^2/3\hat{c}^2$ throughout this paper. The MSSM parameter sets (set 1 to set 7) that we adopt for the figures showing the μ dependences are summarized in Table 2. The two signs of the μ parameter, the two extreme values of $\tan\beta$ (3 and 50), and four values of the lightest chargino mass ($m_{\tilde{\chi}_1^-} = 110, 130, 150$, and 170 GeV) are examined. The \sqrt{s} dependences of the helicity amplitudes are studied in the MSSM parameter sets (set A to set E) given in Table 3. All five cases are for $m_{\tilde{\chi}_1^-} = 110$ GeV, $\tan\beta = 3$, and $\text{sgn}(\mu) = +$. They have different values of the ratio μ/M_2 . The last case (set E) has CP -violating phases φ_1 and φ_μ of M_1 and M_μ , respectively. In Sec. 5.4, we discuss the case of nonzero φ_1 and φ_μ in set E of Table 3.

We show the one-loop contributions of charginos and neutralinos to each helicity amplitude in

	A	B	C	D	E
Parameter					
μ (GeV)	+120	+145	+400	+1000	+130
M_2 (GeV)	541	242	125	115	158
$\tan \beta$	3	3	3	3	3
φ_1	0	0	0	0	$\frac{2}{3}\pi$
φ_μ	0	0	0	0	$\frac{2}{3}\pi$
Mass spectra (GeV)					
$m_{\tilde{\chi}_1^-}$	110	110	110	110	110
$m_{\tilde{\chi}_2^-}$	555	283	420	1007	207
$m_{\tilde{\chi}_1^0}$	99	81	60	57	75
$m_{\tilde{\chi}_2^0}$	123	150	111	110	105
$m_{\tilde{\chi}_3^0}$	285	150	403	1002	154
$m_{\tilde{\chi}_4^0}$	555	285	422	1007	205

Table 3: The parameters and the mass spectrum for the figures of \sqrt{s} dependence. Sets A–D are used in Figs. 3(b), 4(b), and 6(b). Set E is the CP -violating case and used in Figs. 7(a) and 7(b). The lightest chargino mass is fixed to be 110 GeV for all sets.

the form

$$\frac{M_{\tau}^{\lambda\bar{\lambda}}_{\text{MSSM}} - M_{\tau}^{\lambda\bar{\lambda}}_{\text{SM}}}{|M_{\tau}^{\lambda\bar{\lambda}}_{\text{SM}}|}, \quad (5.1)$$

where $M_{\tau}^{\lambda\bar{\lambda}}_{\text{MSSM}}$ are the helicity amplitudes of the MSSM in which only one-loop chargino and neutralino contributions are considered, and $M_{\tau}^{\lambda\bar{\lambda}}_{\text{SM}}$ are those of the SM. From this expression, not only the ratio of the SUSY contributions to the SM amplitude but also its sign (for the real and imaginary parts) can be inferred.

The magnitude and the sign of all the SM amplitudes at the scattering angle $\theta = 90^\circ$ are shown in Fig. 2(a) versus the e^+e^- collision energy \sqrt{s} . Among the tree-level helicity amplitudes, $M_{\tau=-1}^{+-}$, $M_{\tau=-1}^{-+}$, and $M_{\tau=\mp 1}^{00}$ are significant for all energies. The other helicity amplitudes are reduced as \sqrt{s} grows; i.e., $M_{\tau=\pm}^{0\pm}$ and $M_{\tau=\pm}^{\pm 0}$ ($M_{\tau=\pm}^{++}$ and $M_{\tau=\pm}^{--}$) behave as $1/\sqrt{s}$ ($1/s$) [1]. For $\sqrt{s} < 274$ GeV, $M_{\tau=-1}^{0+}$ and $M_{\tau=-1}^{-0}$ are larger than $M_{\tau=-1}^{00}$ at $\cos\theta = 0$. In the following (Secs. 5.1, 5.2, and 5.3), we show the one-loop effects on the helicity amplitudes of $M_{\tau=-1}^{\pm\mp}$, $M_{\tau=\mp 1}^{00}$, and $M_{\tau=-1}^{0+(-0)}$, respectively, in the CP conserving cases. In Sec. 5.4, we examine the loop-induced CP -violating effects on the vertex form factors f_4^Z and f_6^V ($V = \gamma$ and Z) and show their contributions to the helicity amplitudes $M_{\tau=-1}^{0\pm(\mp 0)}$.

In Fig. 2(b), for completeness, the corresponding cross sections integrated for $|\cos\theta| < 0.8$ are shown for each helicity set. The results for the helicity summed total cross section are also shown.

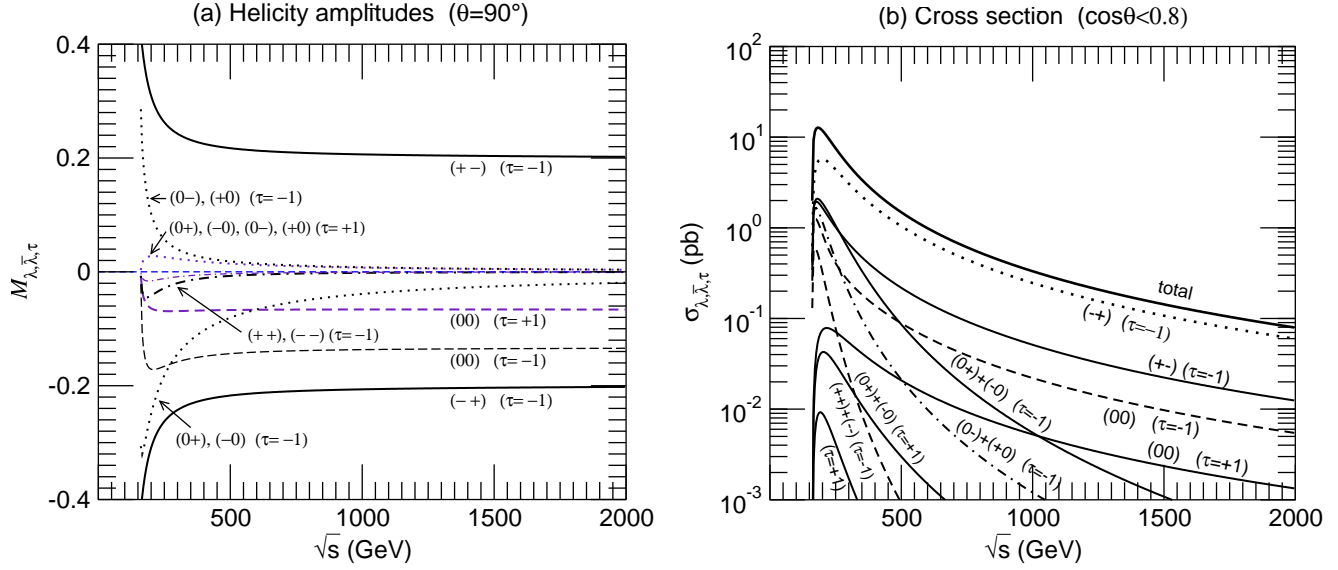


Figure 2: **(a)** The tree-level helicity amplitudes of $e^+e^- \rightarrow W^+W^-$ for each set of $\lambda, \bar{\lambda}$, and τ at the scattering angle 90° . **(b)** The total cross section with $|\cos\theta| < 0.8$ for each helicity set of $\lambda, \bar{\lambda}$, and τ .

5.1 The chargino and neutralino contributions to $M_\tau^{\pm\mp}$

The helicity amplitudes $M_{\tau=-1}^{+-}$ and $M_{\tau=-1}^{-+}$ are the largest of all the helicity amplitudes at large scattering angles. At the tree level, only the t -channel neutrino-exchange diagram contributes to the $(+-)$ and $(-+)$ amplitudes. The one-loop contribution of charginos and neutralinos to these helicity amplitudes comes only from the W -boson wave-function renormalization factor. Therefore, the one-loop effects are essentially independent of the e^+e^- collision energy \sqrt{s} and the scattering angle θ , and they are determined by a logarithmic function of the masses of charginos, neutralinos, and the W boson.

In Fig. 3(a), we show the $|\mu|$ dependence in $M_{\tau=-1}^{+-}$ at the scattering angle $\theta = 90^\circ$. The input parameters are summarized in Table 2. The mass of the lightest chargino is fixed to be 110 GeV for all cases, so that the ratio M_2/μ is a constant for each fixed value of $\tan\beta$ and M_1 . The e^+e^- collision energy \sqrt{s} is set to be at the threshold of the lightest chargino pair production; i.e., $\sqrt{s} = 220$ GeV. In the large $|\mu|$ region, the lightest chargino is Wino-like, i.e., the mass comes from M_2 . We confirmed numerically that in the limit of $\mu \rightarrow \infty$, the deviation becomes constant for μ . This reflects the fact that the lightest chargino is purely Wino-like, and the effect of the Higgsino decouples from the one-loop helicity amplitudes $M_{\tau=-1}^{+-}$ and $M_{\tau=-1}^{-+}$. The deviation at $|\mu| = 1000$ GeV is about 0.08% for set 1–4. For smaller $|\mu|$ values, M_2 becomes larger so that the lightest chargino contribution becomes smaller because of decoupling. On the contrary, for $|\mu|$ around 110 GeV, the lightest chargino is Higgsino-like, i.e., $m_{\tilde{\chi}_1^\pm} \sim |\mu|$. For smaller values of $|\mu|$, a larger Higgsino-like contribution appears. The Wino-like contribution, which is enhanced for the large $|\mu|$ region, and the Higgsino-like contribution, which is substantial for small μ values have the same sign. Therefore, the

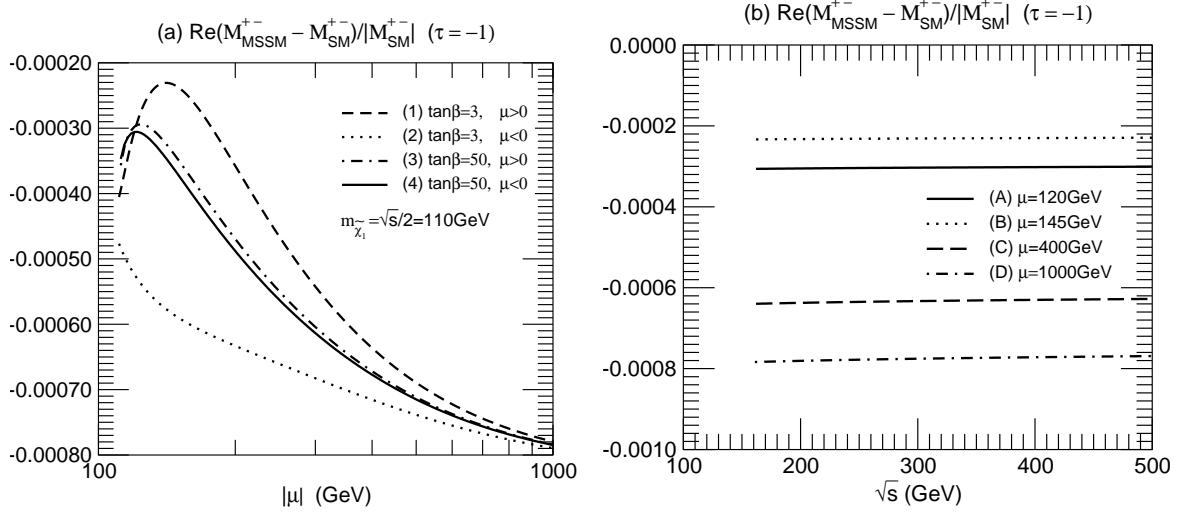


Figure 3: The dependence on (a) $|\mu|$ and (b) \sqrt{s} of the chargino and neutralino one-loop contributions to $M_{\tau=-1}^{+-}$ are shown at $\theta = 90^\circ$ for $m_{\tilde{\chi}_1^-} = 110$ GeV. In Fig. (a), parameters of set 1 to set 4 in Table 2 are used. The e^+e^- collision energy \sqrt{s} is 220 GeV. In Fig. (b), parameters of set A to set D of Table 3 are used.

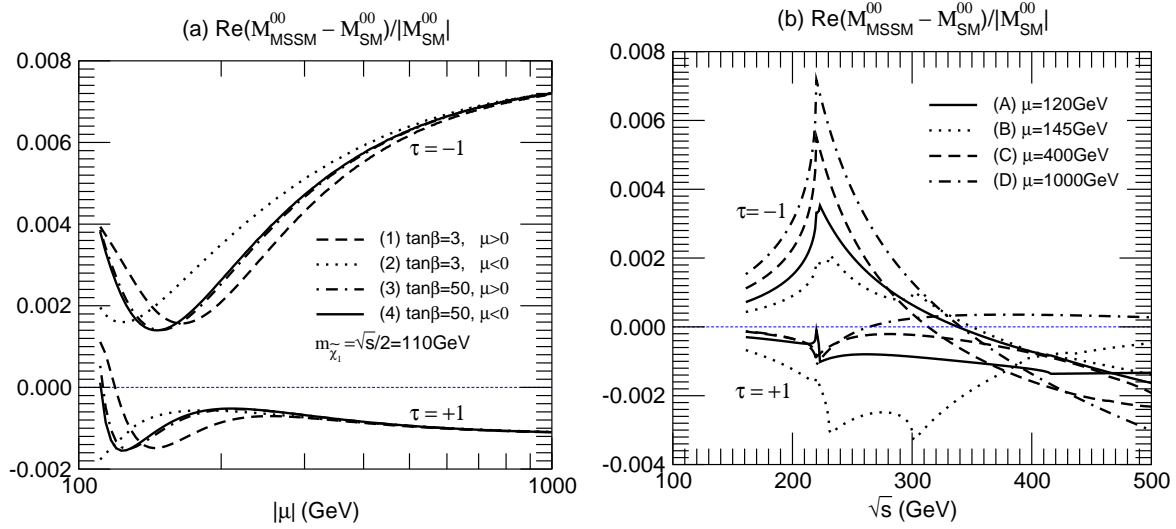


Figure 4: The dependence on (a) $|\mu|$ and (b) \sqrt{s} of the chargino and neutralino one-loop contributions to $M_{\tau=\pm}^{00}$ are shown at $\theta = 90^\circ$ for $m_{\tilde{\chi}_1^-} = 110$ GeV. In Fig. (a), parameters of set 1 to set 4 in Table 2 are used. The e^+e^- collision energy \sqrt{s} is 220 GeV. In Fig. (b), parameters of set A to set D of Table 3 are used.

deviation reaches its minimum at $|\mu| = 140$ GeV for set 1 and $|\mu| = 124$ GeV for set 3 and set 4. For set 2, the deviation monotonically increases, because in this case M_2 is similar to or less than μ even around $\mu = 110$ GeV, so that the Higgsino contribution is smaller than the Wino contribution. The results for set 3 and set 4 are similar, because the mass eigenstates of the chargino and neutralino fields are common between set 3 and set 4 in the limit of large $\tan\beta$.

In Fig. 3(b), $M_{\tau=-1}^{+-}$ is shown as a function of the e^+e^- collider energy \sqrt{s} at $\theta = 90^\circ$ for the parameters of set A to set D in Table 3. The lightest chargino mass is again fixed to be 110 GeV, and μ is assumed to be positive and 120, 145, 400, and 1000 GeV for set A, set B, set C and set D, respectively. The corrections are insensitive to \sqrt{s} , because there is no Feynman diagram of one-loop charginos and neutralinos which contribute to $M_{\tau=-1}^{+-}$. As we do not include the SM one-loop diagrams, the renormalization scale μ_R dependence which comes from the SM running effect in the $\overline{\text{MS}}$ couplings remains in our calculation. By setting μ_R to be \sqrt{s} , an artificial tiny $\ln s$ dependence appears in $M_{\tau=-1}^{+-}$.

The magnitude of the chargino and neutralino contributions to $(+-)$ is small.

5.2 The chargino and neutralino contributions to M_τ^{00}

The one-loop corrections to the trilinear gauge couplings are expected to affect the helicity amplitude M_τ^{00} significantly, because M_τ^{00} includes contributions from s-channel Z boson and photon exchange diagrams.

In Fig. 4(a), we show the effects of charginos and neutralinos on M_τ^{00} ($\tau = \pm$) at $\theta = 90^\circ$ and at the threshold of the lightest chargino-pair production ($\sqrt{s} = 220$ GeV) when $m_{\tilde{\chi}_1^-} = 110$ GeV. The four curves each for $\tau = -1$ and $+1$ correspond to the parameter sets (set 1 to set 4) in Table 2. Like M_τ^{+-} , the Wino effects dominate in the large $|\mu|$ region, while the Higgsino contributes for the small $|\mu|$ region. The effects grow at large values of $|\mu|$ for $\tau = -1$ for all cases, up to about 0.7% at $|\mu| = 1000$ GeV, whereas they remain small for $\tau = +1$, at around the -0.1% level.

In Fig. 4(b), the one-loop contributions of charginos and neutralinos to $M_{\tau=\pm 1}^{00}$ are shown as a function of \sqrt{s} at $\theta = 90^\circ$ for $\tan\beta=3$ and $\mu > 0$. The four sets of parameters (sets A to D) correspond to the different values of $|\mu|$ as listed in Table 3. Let us see the $\tau = -1$ amplitudes first. Sharp peaks can be seen for each curve, which correspond to the thresholds of pair production of the lightest charginos and the two lightest neutralinos. The deviation at the threshold ($\sqrt{s}=220$ GeV) can reach 0.36% for set A, 0.19% for set B, 0.55% for set C, and 0.72% for set D. For $\tau = +1$, the chargino and neutralino corrections from the SM are negative, and hence they interfere constructively with the negative SM amplitude (see Fig. 2(a)). The deviations from the SM prediction at $\sqrt{s}=220$ GeV are 0.0% for set A, -0.15% for set B, and -0.08% for set C and set D. The deviations from the SM are -0.31% at the first threshold of neutralino production and -0.33% at the second threshold of neutralino production for set B. Notice that the tree level amplitude of $M_{\tau=-1}^{00}$ is already twice that of $M_{\tau=+1}^{00}$, so that the one-loop chargino and neutralino contributions to $M_{\tau=-1}^{00}$ at the threshold of light chargino pair production are much larger than those to the $M_{\tau=+1}^{00}$ amplitude.

Finally, in Fig. 5, we show the corrections for different values of the lightest chargino mass as a

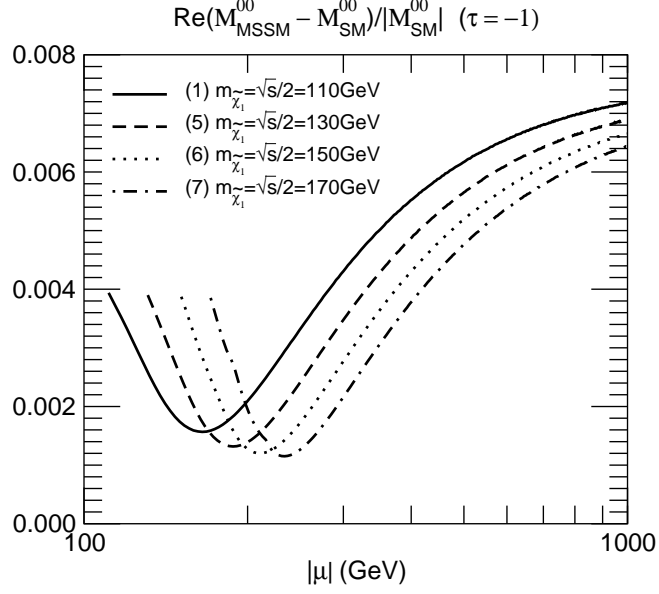


Figure 5: The $|\mu|$ dependences of the chargino and neutralino one-loop contributions to M_τ^{00} are shown for $m_{\tilde{\chi}_1^-} = 110, 130, 150$, and 170 GeV. The e^+e^- collider energy \sqrt{s} is taken to be $2m_{\tilde{\chi}_1^-}$.

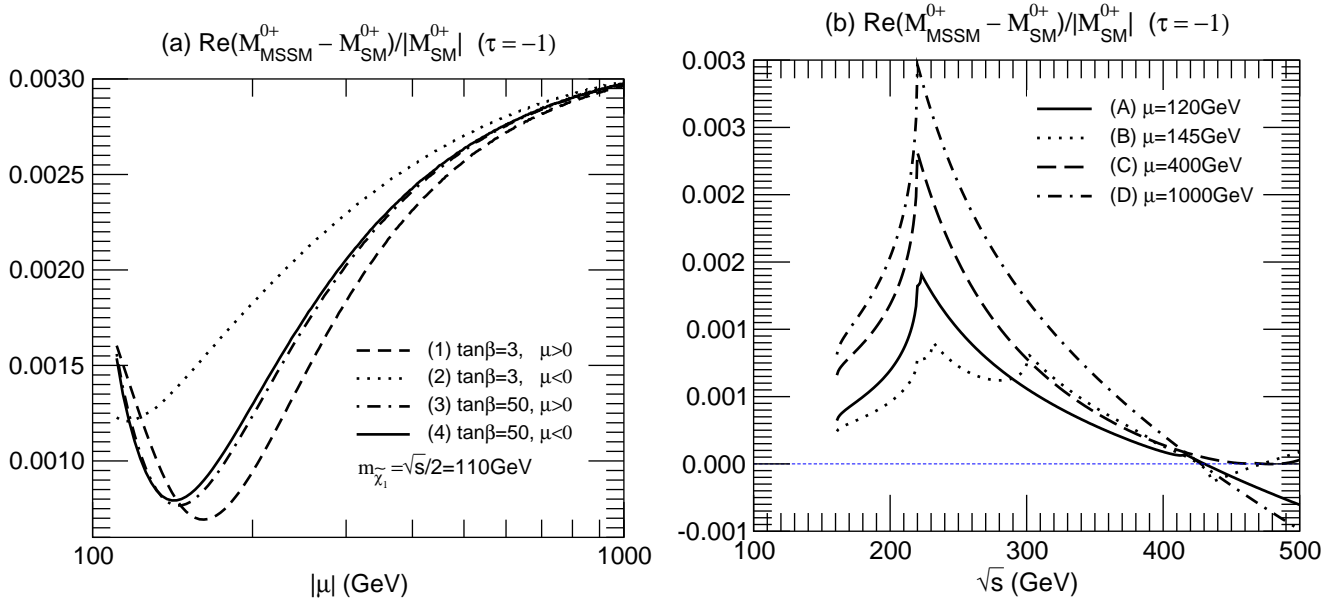


Figure 6: The dependence on (a) $|\mu|$ and (b) \sqrt{s} of the chargino and neutralino one-loop contributions to $M_{\tau=-1}^{0+}$ are shown at $\theta = 90^\circ$ for $m_{\tilde{\chi}_1^-} = 110$ GeV. In Fig. (a), parameters of set 1 to set 4 in Table 2 are used. The e^+e^- collision energy \sqrt{s} is 220 GeV. In Fig. (b), parameters of set A to set D of Table 3 are used.

function of $|\mu|$. The four curves in the figure correspond to set 1, 5, 6, and 7 of Table 2, in which the mass of the lightest charginos are set to be 110, 130, 150, and 170 GeV, respectively. In the large $|\mu|$ region where the lightest chargino is Wino-like, the deviation from the SM value is reduced as $m_{\tilde{\chi}_1^-}$ grows. The deviation at $|\mu| = 1000$ GeV changes from 0.72% to 0.64 % when $m_{\tilde{\chi}_1^-}$ is taken to be 110 GeV (set 1) and 170 GeV (set 7). For smaller values of $|\mu|$ where the lightest chargino is Higgsino-like, the value of the biggest Higgsino contribution at the threshold of the lightest chargino pair production is almost the same for all cases and is about 0.4%.

5.3 The chargino and neutralino contributions to $M_{\tau=-1}^{0+}$ and $M_{\tau=-1}^{-0}$

As already mentioned, the tree-level helicity amplitudes of M_{τ}^{0+} and M_{τ}^{-0} behave as $\mathcal{O}(1/\sqrt{s})$, so that they are substantial only at relatively low energies.

We here present results for the chargino and neutralino one-loop contributions to $M_{\tau=-1}^{0+}$ in Figs. 6(a) and 6(b). We find similar characteristics to the corrections to $M_{\tau=-1}^{00}$, whose details have already been discussed. The magnitude of the deviation from the SM amplitudes is no larger than that of $M_{\tau=-1}^{00}$ for each parameter set at the threshold of light chargino pair production.

5.4 The CP -violating effects

In the general MSSM, there are new CP -violating phases. CP -violating form factors for the $WW\gamma$ and WWZ vertices (f_4^V , f_6^V , and f_7^V with $V = \gamma$ and Z) can be induced beyond the tree level due to the SUSY particle loops.

The CP -violating phases in the chargino and neutralino sectors arise from the μ parameter and the gaugino mass parameters M_1 and M_2 . The other sector of the MSSM Lagrangian also includes CP -violating phases, such as in the gluino mass parameter M_3 and the trilinear A terms of sfermions. The experimental upper bounds on the electric dipole moments (EDM's) of electrons and neutrons provide very severe constraints on those CP -violating phases [13]. It has been found that internal cancellation of the phases in the EDM's may still allow for relatively large CP -violating phases [14]. Large CP -violating phases in the chargino and neutralino sectors are possible without contradicting the EDM constraint, if the parameters for sleptons and squarks of the first generation are adjusted. As we can take the phase of M_2 to be 0 by rephasing, the dependence on the phase of μ (φ_μ) and that of M_1 (φ_1) is examined in this paper. Here, we study the case in which the large CP -violating effects on the $WW\gamma$ and WWZ coupling appear, and examine the deviation in the helicity amplitudes from the CP conserving case. We note that our numerical results in this section are consistent with the result previously obtained by Kitahara et al. [15].

Among the 18 physical form factors of $e^+e^- \rightarrow W^+W^-$ (see Eq. (2,2)), F_4 , F_6 , and F_7 have the CP -odd property. Chargino and neutralino triangle type diagrams for the triple gauge vertices VWW ($V = \gamma$ or Z) contribute to the CP -violating form factors $f_4^{Z(1)}$, $f_6^{\gamma(1)}$, and $f_6^{Z(1)}$ at one loop. We note that the chargino and neutralino loop diagrams do not contribute to $f_7^{V(1)}$, so that F_7 is zero (The relation between the form factors $F_{i,\tau}$ of the $e^+e^- \rightarrow W^+W^-$ amplitude and the form factors f_i^V of the WWV vertices).

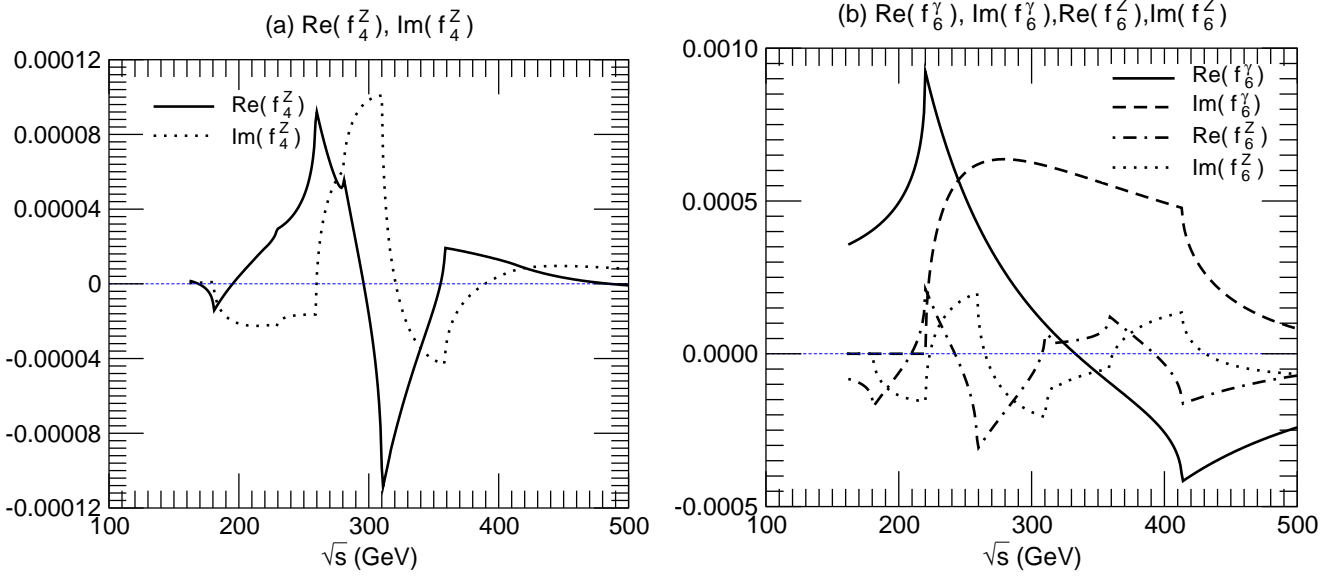


Figure 7: The \sqrt{s} dependences of f_6^γ and f_6^Z are shown for $\varphi_1 = \varphi_\mu = 2\pi/3$. The lightest chargino mass is fixed as 110 GeV and $\mu=130$ GeV. The parameters of set E in Table 3 are used.

In Fig. 7(a), the real part (solid curve) and the imaginary part (dotted curve) of f_4^Z are shown as a function of \sqrt{s} for the parameters of set E in Table 3. The lightest chargino mass is fixed to be 110 GeV, $|\mu|$ is 130 GeV, and $\tan\beta = 3$. The CP -violating phases φ_1 and φ_μ are taken to be $2\pi/3$. The threshold of the neutralino pair production for $\tilde{\chi}_1^0\tilde{\chi}_2^0$, $\tilde{\chi}_1^0\tilde{\chi}_3^0$, $\tilde{\chi}_2^0\tilde{\chi}_3^0$, $\tilde{\chi}_1^0\tilde{\chi}_4^0$, $\tilde{\chi}_2^0\tilde{\chi}_4^0$, or $\tilde{\chi}_3^0\tilde{\chi}_4^0$ is located at $\sqrt{s} = 180, 229, 259, 280$, or 310 GeV, respectively. The real part has a peak at each threshold, while the imaginary part shows a rapid s -wave rise above the threshold. The magnitude of $\text{Re}(f_4^Z)$ and $\text{Im}(f_4^Z)$ is small and is at most 10^{-4} .

The \sqrt{s} dependences of the real part and the imaginary part of f_6^γ and f_6^Z are shown in Fig. 7(b) for the same parameter choice as in Fig. 7(a); i.e., set E of Table 3. The solid and dashed curves correspond to $\text{Re}(f_6^\gamma)$ and $\text{Im}(f_6^\gamma)$, while the dot-dashed and dotted curves represent $\text{Re}(f_6^Z)$ and $\text{Im}(f_6^Z)$, respectively. In the one-loop triangle diagrams for $\gamma W^+ W^-$, only the chargino loops appear with the diagonal vertices $\gamma\tilde{\chi}_i^-\tilde{\chi}_i^+$ ($i = 1, 2$), so that the threshold effects for $\tilde{\chi}_1^+\tilde{\chi}_1^-$ and $\tilde{\chi}_2^+\tilde{\chi}_2^-$ pair production are seen at 220 and 414 GeV, respectively. At the lightest chargino pair production threshold, the magnitude of $\text{Re}(f_6^\gamma)$ can reach about 10^{-3} . We note that at $\sqrt{s} = 220$ GeV the maximal value of $f_6^{\gamma(1)}$ strongly depends on $\tan\beta$; it is 0.0017, 0.0013, or 0.00027 for $\tan\beta = 1, 2$, and 10, respectively. For larger $\tan\beta$, smaller values of $f_6^{\gamma(1)}$ are obtained. On the other hand, f_6^Z shows more complicated behavior due to the threshold structure of neutralino pairs as well as chargino pairs. The magnitude of the real part is $-1.7 (+2.4, -3.2) \times 10^{-4}$ at the threshold of $\tilde{\chi}_1^0\tilde{\chi}_2^0$ ($\tilde{\chi}_1^+\tilde{\chi}_1^-, \tilde{\chi}_2^0\tilde{\chi}_3^0$). The dotted line is the imaginary part of f_6^Z . The magnitude of the imaginary part is as large as that of the real part.

In Fig. 8, contour plots of (a) $\text{Re}(f_6^Z)$, (b) $\text{Im}(f_6^Z)$, (c) $\text{Re}(f_6^\gamma)$, and (d) $\text{Im}(f_6^\gamma)$ are shown in the

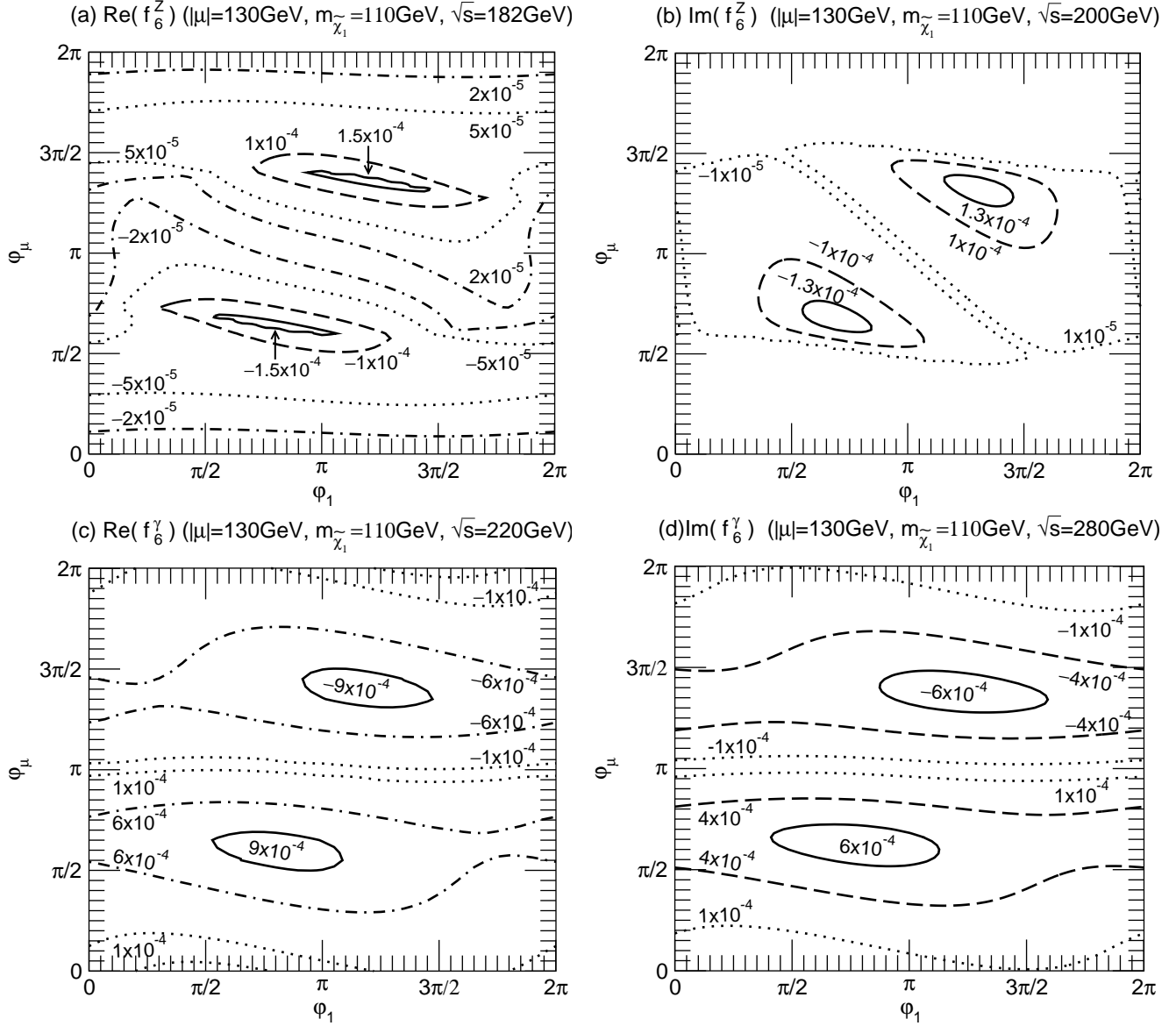


Figure 8: The contour plots of f_6^γ and f_6^Z are shown in the φ_1 - φ_μ plane. The e^+e^- collision energy \sqrt{s} is taken to be 182, 200, 220, and 280 GeV for $\text{Re}(f_6^Z)$, $\text{Im}(f_6^Z)$, $\text{Re}(f_6^\gamma)$, and $\text{Im}(f_6^\gamma)$, respectively. The lightest chargino mass $m_{\tilde{\chi}_1^-}$ is fixed as 110 GeV, and $|\mu|$ is taken to be 130 GeV.

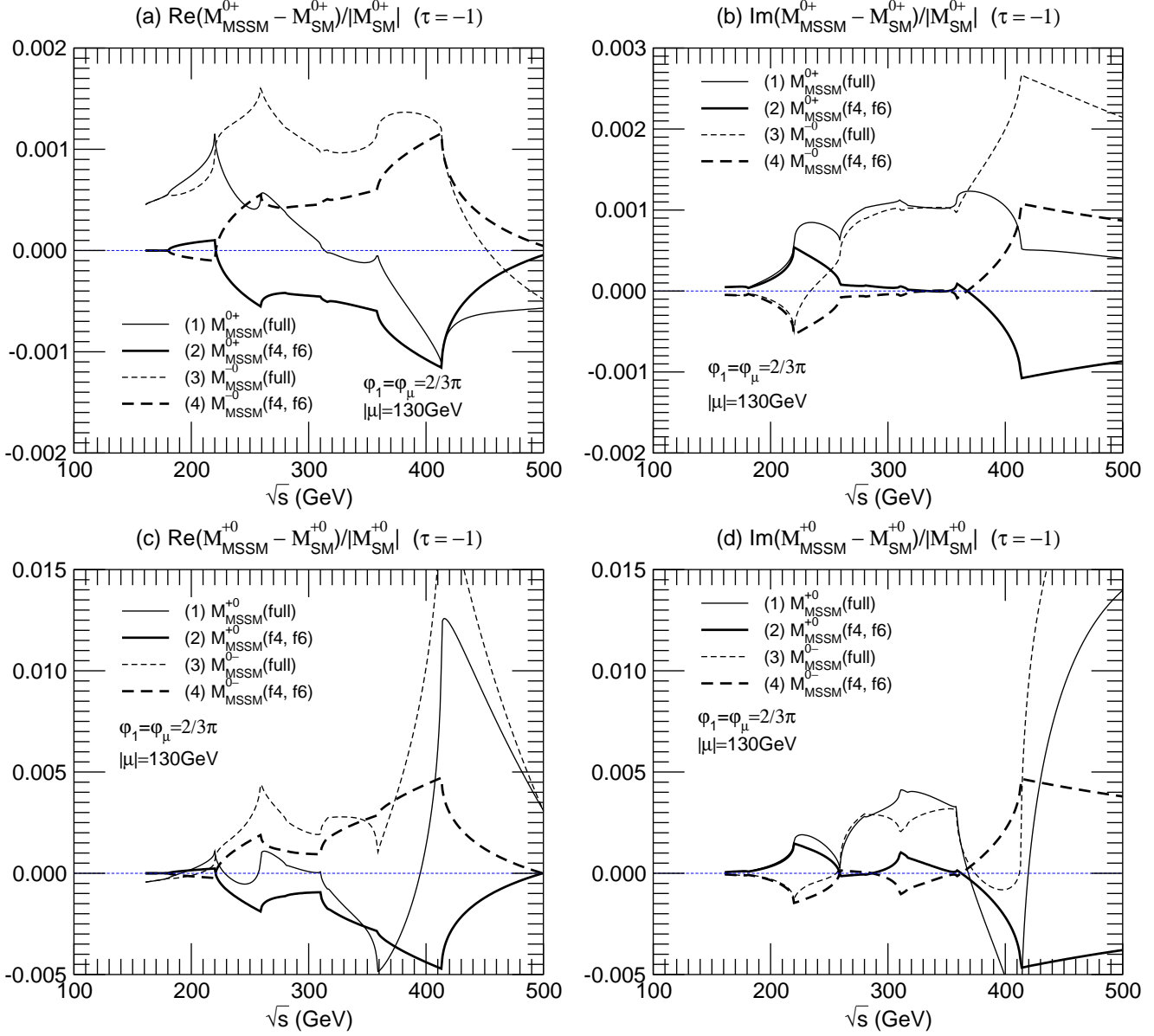


Figure 9: The \sqrt{s} dependences of the chargino and neutralino contributions to the real part and the imaginary part of $M_{\tau=-1}^{0+}$, $M_{\tau=-1}^{-0}$, $M_{\tau=-1}^{+0}$, and $M_{\tau=-1}^{0-}$ are shown at $\theta = 90^\circ$ for $m_{\tilde{\chi}_1^-} = 110$ GeV. The CP phases φ_1 and φ_μ are set to be $2/3\pi$. $|\mu|$ is fixed to be 130 GeV. The parameters of set E in Table 3 is used. The helicity amplitude $M_{\text{MSSM}}(\text{full})$ contains contributions from all form factors, while $M_{\text{MSSM}}(\text{f4, f6})$ includes only the contributions from the form factors F_4 and F_6 .

φ_1 - φ_μ plane. The lightest chargino mass is fixed as 110 GeV. We have chosen $|\mu|$ to be 130 GeV, where relatively large values of f_6^γ and f_6^Z are observed. The relation $|M_1| = |M_2|5\hat{s}^2/3\hat{c}^2$ is used even though we allow M_1/M_2 to have an arbitrary phase φ_1 . The value of M_2 is set so as to give the mass of the lightest chargino to be 110 GeV with $\tan\beta=3$. We also choose \sqrt{s} to be 182, 200, 220, and 280 GeV for the figures of $\text{Re}(f_6^Z)$, $\text{Im}(f_6^Z)$, $\text{Re}(f_6^\gamma)$, and $\text{Im}(f_6^\gamma)$, respectively, where the form factors are relatively large (See Figs. 7(a) and 7(b)). φ_1 and φ_μ are allowed to vary between 0 and 2π . As shown in the figures, both f_6^Z and f_6^γ take their maximum or minimum at around $\varphi_1 = \varphi_\mu = 2\pi/3$ or $4\pi/3$. $\text{Re}(f_6^Z)$ ($\text{Im}(f_6^Z)$) can be 1.5 (1.3) $\times 10^{-4}$, while $\text{Re}(f_6^\gamma)$ ($\text{Im}(f_6^\gamma)$) can be larger than 9.0 (6.0) $\times 10^{-4}$.

In Figs. 9(a) to 9(d), we show the effects of nonzero f_4^Z and $f_6^{Z,\gamma}$ on the helicity amplitude of M^{0+} , M^{-0} , M^{+0} and M^{0-} (see Eqs. (2.3c) and (2.3b)). In Fig. 9(a) (9(b)), the real (imaginary) part of the deviation in M^{0+} , and M^{-0} with $\tau = -1$ from the SM prediction is shown for (1 and 3) the full one-loop chargino and neutralino effects and (2 and 4) only the effects from f_4 and f_6 . Similarly, in Fig. 9(c) (9(d)), the real (imaginary) part of the deviation in M^{+0} and M^{0-} is shown for (1 and 3) the full one-loop chargino and neutralino effects and (2 and 4) only the effects from f_4 and f_6 . We note that the pure effect of the CP -violation can be measured by the difference between $M_\tau^{\pm 0}$ and $M_\tau^{0\mp}$:

$$M_\tau^{\pm 0} - M_\tau^{0\mp} = -i\sqrt{2}s\gamma\tau [\beta F_{4,\tau} \mp F_{6,\tau}]. \quad (5.2)$$

As shown in Figs. 9(a) and 9(b) (9(c) and 9(d)), the CP -violating effect $M_{\text{MSSM}}^{0+} - M_{\text{MSSM}}^{-0}$ ($M_{\text{MSSM}}^{+0} - M_{\text{MSSM}}^{0-}$) can be of the order of 0.1% (a few times 0.1%) as compared to the size of $|M_{\text{SM}}^{0+}(\tau = -1)|$ ($|M_{\text{SM}}^{+0}(\tau = -1)|$) just after the threshold of the lightest chargino-pair production. The correction to M^{+0} (or M^{0-}) is larger than that to M^{0+} (or M^{-0}), because the SM value for the former is smaller than for the latter.

6 Discussion and Conclusion

In this paper, we have studied one-loop contributions of charginos and neutralinos to the helicity amplitudes of $e^+e^- \rightarrow W^+W^-$ in the MSSM.

The form factors are calculated at one loop in the $\overline{\text{MS}}$ scheme. In order to establish the validity of our one-loop calculation, we tested the one-loop form factors by using the BRS sum rules among the form factors between $e^+e^- \rightarrow W^+W^-$ and $e^+e^- \rightarrow \omega^+W^-$. Furthermore, overall factors such as the wave-function renormalization factor, which cannot be tested by the BRS sum rules, are tested by the use of the decoupling property of the SUSY particles in the large soft-breaking mass limit. As pointed out in Ref. [1], this procedure for testing the one-loop calculation works well when we reexpand the one-loop expression of the form factors by the $\overline{\text{MS}}$ couplings of the SM and truncate the higher order terms. These tests at the numerical level ensure the consistency of our one-loop calculation scheme and our numerical program.

The use of the SM $\overline{\text{MS}}$ coupling constants as expansion parameters for our perturbation calculation is valid around and below the thresholds of the light SUSY particle pair production. However we

have adopted this calculation scheme for even higher energy scales, where the original $\overline{\text{MS}}$ scheme with the MSSM coupling constants should be more appropriate for the resummation of logarithmic terms of the type $\ln s/m_{\text{SUSY}}^2$. In Ref. [1], we evaluated the error of our calculational scheme at high energies in the case of sfermion loop contributions. The numerical difference in $M_{\tau=-1}^{00}$ between our scheme and the usual $\overline{\text{MS}}$ scheme is at most around 0.01% for energies below a few TeV.

We have not included the one-loop diagrams for the SM particles in our calculation. We have shown most of our results as a deviation from the SM prediction.

For numerical evaluation of the helicity amplitudes, the SUSY parameters in the chargino and neutralino sectors are chosen so as to satisfy the constraints from the current experimental data; i.e., results from electroweak precision measurements at the Tevatron and LEP2, direct search results for the chargino and neutralino at LEP2, as well as the current EDM data. Under these constraints, we took the mass of the lightest chargino as light as possible to obtain large corrections.

In the CP conserving case, we showed results for the chargino and neutralino contributions to the helicity amplitudes M_{τ}^{+-} , M_{τ}^{00} , and M_{τ}^{0+} . Like the sfermion loop effect, the amplitude for the mode of the longitudinally polarized W -boson pair production $M_{\tau=-1}^{00}$ is found to be the most useful to study the chargino and neutralino contributions, having relatively large loop effects as compared to those for other helicity sets. Unlike the sfermion loop effects given in Ref. [1], the enhancement at each threshold of the chargino- or neutralino-pair production is sharp because of the s -wave nature of the fermion-pair production threshold. The corrections to the SM prediction for the helicity amplitude $M_{\tau=-1}^{00}$ can be as large as -0.7% at the threshold of the lightest chargino-pair production for large scattering angles. Therefore, we found that the typical value of the chargino and neutralino contribution is larger than that of the sfermion contribution.

We also studied the effects of CP -violating phases in the chargino and neutralino sectors on the helicity amplitudes. The CP -violating factors f_4^Z and f_6^V ($V = \gamma$ and Z) of the VW^+W^- vertices are induced at one-loop level due to the triangle diagrams of charginos and neutralinos. Another CP -violating factors f_7^V are not induced from these diagrams and remains zero. The size of the loop-induced form factors $f_4^{Z(1)}$ and $f_6^{V(1)}$ can be of the order of 10^{-3} when the CP -violating phases of the chargino and neutralino sectors are around $\varphi_1 \simeq \varphi_\mu \simeq 2\pi/3$ and $4\pi/3$ for $|\mu| = 130$ GeV. These loop-induced CP -violating form factors $f_4^{(1)Z}$ and $f_6^{(1)V}$ can affect the helicity amplitudes $M_{\tau=-1}^{0\pm}$ and $M_{\tau=-1}^{\mp 0}$. In particular, for a large scattering angle ($\cos\theta \simeq 0$), the difference $M_{\tau=-1}^{0\pm} - M_{\tau=-1}^{\mp 0}$ measures the pure CP -violating effect from $f_4^{Z(1)}$ and $f_6^{V(1)}$. We find that the CP -violating effect on $M_{\tau=-1}^{0+} - M_{\tau=-1}^{0-}$ ($M_{\tau=-1}^{0-} - M_{\tau=-1}^{0+}$) in the chargino and neutralino sectors can be as large as a few times 0.1% of the SM prediction for $M_{\tau=-1}^{0+}$ ($M_{\tau=-1}^{0-}$).

In conclusion, the correction from the chargino and neutralino contributions to $e^+e^- \rightarrow W^+W^-$ can be as large as $\mathcal{O}(1\%)$ in amplitude, which is much larger than that of the sfermion contribution. The loop-induced CP -violating effects from the phases in the chargino and neutralino sectors can provide corrections of $\mathcal{O}(0.1\%)$ in amplitude.

Acknowledgments

Y.U. acknowledges the support of BMBF, contract No. 05 HT1PAA 4. M.K. was supported by DFG under Contract No. KL 1266/1-3.

A The Lagrangian

In this paper we are concerned with the chargino and neutralino contributions to one-loop $e^+e^- \rightarrow W^+W^-$ amplitudes. The purpose of this appendix is to provide all masses, mixing angles, and couplings that are required to reproduce and use our results. We begin by discussing the chargino and neutralino mass matrices. We will consider two CP -violating phases of the μ parameter and the gaugino mass M_1 , which are denoted φ_μ and φ_1 , respectively.

A.1 Chargino mass eigenstates

The chargino mass term is given by

$$-\mathcal{L} = \begin{pmatrix} \overline{\widetilde{W}_R^-} & \overline{\widetilde{H}_{uR}^-} \end{pmatrix} M_C \begin{pmatrix} \widetilde{W}_L^- \\ \widetilde{H}_{dL}^- \end{pmatrix} + \text{h.c.} , \quad (\text{A.1})$$

where the mass matrix is defined by

$$M_C = \begin{pmatrix} M_2 & \sqrt{2}m_W c_\beta \\ \sqrt{2}m_W s_\beta & \mu e^{i\varphi_\mu} \end{pmatrix} . \quad (\text{A.2})$$

The matrix M_C can be diagonalized by using two unitary matrices

$$U_R^{C\dagger} M_C U_L^C = \text{diag}(m_{\widetilde{\chi}_1^-}, m_{\widetilde{\chi}_2^-}) , \quad (\text{A.3})$$

where the chargino mass $m_{\widetilde{\chi}_i^-}$ is real and positive and has the relation $m_{\widetilde{\chi}_1^-} < m_{\widetilde{\chi}_2^-}$.

The mass eigenstates are defined by

$$\widetilde{\chi}_i^- = \widetilde{\chi}_{iL}^- + \widetilde{\chi}_{iR}^- , \quad (\text{A.4})$$

where

$$\begin{pmatrix} \overline{\widetilde{W}_L^-} \\ \overline{\widetilde{H}_{dL}^-} \end{pmatrix} = U_L^C \begin{pmatrix} \widetilde{\chi}_{1L}^- \\ \widetilde{\chi}_{2L}^- \end{pmatrix} , \quad \begin{pmatrix} \overline{\widetilde{W}_R^-} \\ \overline{\widetilde{H}_{uR}^-} \end{pmatrix} = U_R^C \begin{pmatrix} \widetilde{\chi}_{1R}^- \\ \widetilde{\chi}_{2R}^- \end{pmatrix} . \quad (\text{A.5})$$

The mass term (A.1) is now expressed as

$$-\mathcal{L} = \begin{pmatrix} \overline{\widetilde{\chi}_{1R}^-} & \overline{\widetilde{\chi}_{2R}^-} \end{pmatrix} U_R^{C\dagger} M_C U_L^C \begin{pmatrix} \widetilde{\chi}_{1L}^- \\ \widetilde{\chi}_{2L}^- \end{pmatrix} + \text{h.c.} = \sum_{i=1}^2 m_{\widetilde{\chi}_i^-} \left(\overline{\widetilde{\chi}_{iR}^-} \widetilde{\chi}_{iL}^- + \text{h.c.} \right) = \sum_{i=1}^2 m_{\widetilde{\chi}_i^-} \overline{\widetilde{\chi}_i^-} \widetilde{\chi}_i^- . \quad (\text{A.6})$$

A.2 Neutralino mass eigenstates

The neutralino mass term is given by

$$-\mathcal{L} = \frac{1}{2} \begin{pmatrix} \widetilde{B}_R & \widetilde{W}_R^3 & \widetilde{H}_{dR}^0 & \widetilde{H}_{uR}^0 \end{pmatrix} M_N \begin{pmatrix} \widetilde{B}_L \\ \widetilde{W}_L^3 \\ \widetilde{H}_{dL}^0 \\ \widetilde{H}_{uL}^0 \end{pmatrix} + \text{h.c.} , \quad (\text{A.7})$$

where the mass matrix is defined by

$$M_C = \begin{pmatrix} M_1 e^{i\varphi_1} & 0 & -m_Z s_W c_\beta & +m_Z s_W s_\beta \\ 0 & M_2 & +m_Z c_W c_\beta & -m_Z c_W s_\beta \\ -m_Z s_W c_\beta & +m_Z c_W c_\beta & 0 & -\mu e^{i\varphi_\mu} \\ +m_Z s_W s_\beta & -m_Z c_W s_\beta & -\mu e^{i\varphi_\mu} & 0 \end{pmatrix}. \quad (\text{A.8})$$

The matrix M_N can be diagonalized by using two unitary matrices

$$U_R^{N\dagger} M_C U_L^N = \text{diag}(m_{\tilde{\chi}_1^0}, m_{\tilde{\chi}_2^0}, m_{\tilde{\chi}_3^0}, m_{\tilde{\chi}_4^0}). \quad (\text{A.9})$$

Because the neutralinos are Majorana fermions, the mass matrix M_N is symmetric ($M_N^T = M_N$). Therefore the two unitary matrices U_L^N and U_R^N can be chosen the same, except for the phase matrix which makes the neutralino mass real and positive:

$$U_L^N = U_N P_N^*, U_R^N = U_N^* P_N, P_N = \text{diag}(e^{i\xi_1/2}, e^{i\xi_2/2}, e^{i\xi_3/2}, e^{i\xi_4/2}), \quad (\text{A.10})$$

where P_N is the phase matrix. The mass eigenstates are given by

$$\tilde{\chi}_i^0 = \tilde{\chi}_{iL}^0 + \tilde{\chi}_{iR}^0. \quad (\text{A.11})$$

The current eigenstates

$$X_{Li} = (\widetilde{B}_L, \widetilde{W}_L^3, \widetilde{H}_{dL}^0, \widetilde{H}_{uL}^0), \quad X_{Ri} = (\widetilde{B}_R, \widetilde{W}_R^3, \widetilde{H}_{dR}^0, \widetilde{H}_{uR}^0), \quad (\text{A.12})$$

are now expressed in terms of the mass eigenstates $\tilde{\chi}_{iL}^0$ and $\tilde{\chi}_{iR}^0$, respectively, by

$$X_{Li} = (U_L^N)_{ij} \tilde{\chi}_{jL}^0, \quad X_{Ri} = (U_R^N)_{ij} \tilde{\chi}_{jR}^0. \quad (\text{A.13})$$

It is worth noting here that with the above phase convention the mass-eigenstate neutralino fields satisfy the Majorana condition

$$(\tilde{\chi}_{iL}^0)^c = \tilde{\chi}_{iR}^0, \quad (\text{A.14})$$

and hence for the four-component Majorana fields

$$(\tilde{\chi}_i^0)^c = \tilde{\chi}_i^0. \quad (\text{A.15})$$

A.3 Chargino–gauge boson and neutralino–gauge boson interaction

The interactions of gauge bosons with charginos and neutralinos are given by

$$\mathcal{L}_{V\widetilde{\chi}\widetilde{\chi}} = g_{\alpha}^{\widetilde{\chi}_1\widetilde{\chi}_2V}\overline{\widetilde{\chi}_1}\gamma^{\mu}P_{\alpha}\widetilde{\chi}_2V_{\mu}, \quad (\text{A.16})$$

where $\chi = \chi^0$ and χ^- and $V_{\mu} = \gamma_{\mu}$ and Z_{μ} are implied. The couplings of the chargino-neutralino-gauge boson interaction are given by

$$g_L^{\widetilde{\chi}_i^0\widetilde{\chi}_j^-W} = (g_L^{\widetilde{\chi}_j^-\widetilde{\chi}_i^0W})^* = -g \left\{ (U_L^N)_{2i}^*(U_L^C)_{1j} + \frac{1}{\sqrt{2}}(U_L^N)_{3i}^*(U_L^C)_{2j} \right\}, \quad (\text{A.17a})$$

$$g_R^{\widetilde{\chi}_i^0\widetilde{\chi}_j^-W} = (g_R^{\widetilde{\chi}_j^-\widetilde{\chi}_i^0W})^* = -g \left\{ (U_R^N)_{2i}^*(U_R^C)_{1j} - \frac{1}{\sqrt{2}}(U_R^N)_{4i}^*(U_R^C)_{2j} \right\}. \quad (\text{A.17b})$$

The couplings of the chargino-chargino-gauge boson interaction are given by

$$g_L^{\widetilde{\chi}_i^-\widetilde{\chi}_j^-Z} = g_Z \left\{ (U_L^C)_{1i}^*(U_L^C)_{1j} + \frac{1}{2}(U_L^C)_{2i}^*(U_L^C)_{2j} - s_W^2\delta_{ij} \right\}, \quad (\text{A.18a})$$

$$g_R^{\widetilde{\chi}_i^-\widetilde{\chi}_j^-Z} = g_Z \left\{ (U_R^C)_{1i}^*(U_R^C)_{1j} + \frac{1}{2}(U_R^C)_{2i}^*(U_R^C)_{2j} - s_W^2\delta_{ij} \right\}, \quad (\text{A.18b})$$

$$g_L^{\widetilde{\chi}_i^-\widetilde{\chi}_i^-A} = g_R^{\widetilde{\chi}_i^-\widetilde{\chi}_i^-A} = e. \quad (\text{A.18c})$$

The couplings of the neutralino-neutralino-gauge boson interaction are given by

$$g_L^{\widetilde{\chi}_i^0\widetilde{\chi}_j^0Z} = -\frac{1}{2}g_Z \left\{ (U_L^N)_{3i}^*(U_L^N)_{3j} - (U_L^N)_{4i}^*(U_L^N)_{4j} \right\}, \quad g_R^{\widetilde{\chi}_i^0\widetilde{\chi}_j^0Z} = -g_L^{\widetilde{\chi}_j^0\widetilde{\chi}_i^0Z}. \quad (\text{A.19})$$

The interaction with charge conjugated fermions of Eq. (A.16) can be rewritten by

$$\mathcal{L} = g_{\alpha}^{\widetilde{\chi}_1^c\widetilde{\chi}_2^cV}\overline{\widetilde{\chi}_1^c}\gamma^{\mu}P_{\alpha}\widetilde{\chi}_2^cV_{\mu}, \quad (\text{A.20})$$

where the coupling $g_{\alpha}^{\widetilde{\chi}_1^c\widetilde{\chi}_2^cV}$ is related to the coupling $g_{\alpha}^{\widetilde{\chi}_1\widetilde{\chi}_2V}$ by

$$g_L^{\widetilde{\chi}_1^c\widetilde{\chi}_2^cV} = -g_R^{\widetilde{\chi}_2\widetilde{\chi}_1V}, \quad g_R^{\widetilde{\chi}_1^c\widetilde{\chi}_2^cV} = -g_L^{\widetilde{\chi}_2\widetilde{\chi}_1V}. \quad (\text{A.21})$$

The minus sign arises because of the charge conjugation of the vector current.

A.4 Chargino–Goldstone boson and neutralino–Goldstone boson interaction

The interactions of the Goldstone boson with charginos and neutralinos are given by

$$\mathcal{L}_{\omega\widetilde{\chi}\widetilde{\chi}} = g_{\alpha}^{\widetilde{\chi}_1\widetilde{\chi}_2\omega}\overline{\widetilde{\chi}_1}P_{\alpha}\widetilde{\chi}_2\omega. \quad (\text{A.22})$$

The chargino-neutralino-Goldstone boson couplings are given by

$$g_L^{\widetilde{\chi}_i^0\widetilde{\chi}_j^-\omega^-} = (g_R^{\widetilde{\chi}_j^-\widetilde{\chi}_i^0\omega^-})^* = -i\frac{g}{\sqrt{2}} \left\{ (U_R^N)_{2i}^*(U_L^C)_{2j} - \sqrt{2}(U_R^N)_{3i}^*(U_L^C)_{1j} + t_W(U_R^N)_{1i}^*(U_L^C)_{2j} \right\} \cos \beta, \quad (\text{A.23a})$$

$$g_R^{\widetilde{\chi}_i^0\widetilde{\chi}_j^-\omega^-} = (g_L^{\widetilde{\chi}_j^-\widetilde{\chi}_i^0\omega^-})^* = -i\frac{g}{\sqrt{2}} \left\{ (U_L^N)_{2i}^*(U_R^C)_{2j} + \sqrt{2}(U_L^N)_{4i}^*(U_R^C)_{1j} + t_W(U_L^N)_{1i}^*(U_R^C)_{2j} \right\} \sin \beta. \quad (\text{A.23b})$$

i	1	2	3	4	5	6	7	8	9	10	11	12	13	14	15	16
$f_i^{\gamma(0)}$	1		2							-1			1			
$f_i^{Z(0)}$	1		2							-1			1			
$f_i^{t(0)}$	1		2		1			1		-2			2			

Table 4: Explicit values for $f_i^{\gamma(0)}$, $f_i^{Z(0)}$, and $f_i^{t(0)}$ in Eq. (B.1). Only nonzero values are shown.

The interaction with charge conjugated fermions of Eq. (A.22) can be rewritten as

$$\mathcal{L} = g_{\alpha}^{\tilde{\chi}_1^c \tilde{\chi}_2^c \omega} \overline{\tilde{\chi}_1^c} P_{\alpha} \tilde{\chi}_2^c \omega , \quad (\text{A.24})$$

where the coupling $g_{\alpha}^{\tilde{\chi}_1^c \tilde{\chi}_2^c \omega}$ is related to the coupling $g_{\alpha}^{\tilde{\chi}_1 \tilde{\chi}_2 \omega}$ by

$$g_L^{\tilde{\chi}_1^c \tilde{\chi}_2^c V} = g_L^{\tilde{\chi}_2 \tilde{\chi}_1 V} , \quad g_R^{\tilde{\chi}_1^c \tilde{\chi}_2^c V} = g_R^{\tilde{\chi}_2 \tilde{\chi}_1 V} . \quad (\text{A.25})$$

B Chargino and neutralino effects on the form factors

B.1 Form factors $\tilde{F}_{i,\tau}$ and $F_{i,\tau}^{(1)\text{ext}}$

The $\tilde{F}_{i,\tau}$ are expressed by

$$\begin{aligned} \tilde{F}_{i,\tau}(s, t) = & \frac{\hat{e}^2}{s} \left\{ \left[Q_e \left(1 - \Pi_{T,\gamma}^{\gamma\gamma}(s) + \Gamma_1^e(s) \right) + T_e^3 \overline{\Gamma}_2^e(s) \right] f_i^{\gamma(0)} + Q_e f_i^{\gamma(1)}(s) \right\} \\ & + \frac{\hat{g}^2}{s - (m_W^2/\hat{c}^2)} \left\{ \left[(T_e^3 - \hat{s}^2 Q_e) \left(1 + \frac{\Delta}{s - m_W^2/\hat{c}^2} - \Pi_{T,Z}^{ZZ}(s) + \Gamma_1^e(s) \right) + T_e^3 \left(\hat{c}^2 \overline{\Gamma}_2^e(s) + \Gamma_3^e(s) \right) \right. \right. \\ & \quad \left. \left. + \Gamma_4^e(s) \right] f_i^{Z(0)} + (T_e^3 - \hat{s}^2 Q_e) f_i^{Z(1)}(s) - \frac{\hat{s}}{\hat{c}} \left[Q_e \hat{c}^2 f_i^{Z(0)} + (T_e^3 - \hat{s}^2 Q_e) f_i^{\gamma(0)} \right] \Pi_{T,\gamma}^{\gamma Z}(s) \right\} \\ & + \frac{T_e^3 \hat{g}^2}{2t} \left[f_i^{t(0)} + \Gamma^{e\nu W}(t) + \overline{\Gamma}^{e\nu W}(t) \right] + F_{i,\tau}^{[\text{Box}]}(s, t) , \end{aligned} \quad (\text{B.1})$$

where $i = 1 - 16$. The two-point functions $\Pi_{T,\gamma}^{\gamma\gamma}$, $\Pi_{T,\gamma}^{ZZ}$, and $\Pi_{T,Z}^{ZZ}$ are given in Appendix B 3.

The vertex coefficients f_i^V are divided into the tree contribution and the one-loop vertex contribution according to Eq. (3.7),

$$f_i^V(s) = f_i^{V(0)} + f_i^{V(1)}(s) , \quad (\text{B.2})$$

where $V = \gamma$ and Z . The nonzero tree-level values $f_i^{V(0)}$ are given in Table 4. The vertex functions for the Vee vertex, denoted by Γ_1^e , $\overline{\Gamma}_2^e$, Γ_3^e , and Γ_4^e , also appear in the $e^- e^+ \rightarrow f \bar{f}$ amplitudes [11]. The vertex functions $\Gamma^{e\nu W}$ and $\overline{\Gamma}^{e\nu W}$ appear in charged current processes; they contain $\nu e W$ vertex corrections as well as two-point function corrections for the external electrons and W bosons and the internal neutrino propagator. Finally, the $F_{i,\tau}^{[\text{Box}]}$ terms account for contributions of box diagrams. In the limit of heavy SUSY particles except for the chargino and neutralino that we study in this

paper, all these vertex functions $\Gamma_1^e, \bar{\Gamma}_2^e, \Gamma_3^e, \Gamma_4^e, \Gamma^{\nu W}$, and $\bar{\Gamma}^{\nu W}$ and the box corrections are small and we can set them to zero.

Next, for the part of the corrections to external W -boson lines, $F_{i,\tau}^{(1)\text{ext}}$, we have only to discuss the cases in which all the external W bosons are physical (λ or $\bar{\lambda} = 0, \pm 1$);

$$F_{i,\tau}^{(1)\text{ext}}(s, t) = \left[\frac{\hat{e}^2}{s} Q_e f_i^{\gamma(0)} + \frac{\hat{g}^2}{s - (m_W^2/\hat{c}^2)} (T_e^3 - \hat{s}^2 Q_e) f_i^{Z(0)} + \frac{T_e^3 \hat{g}^2}{2t} f_i^{t(0)} \right] \delta Z_W, \quad (\text{B.3})$$

where $i = 1 - 9$ and δZ_W is the wave-function renormalization factor of physical W bosons with helicities λ or $\bar{\lambda} = 0, \pm$, and its chargino and neutralino one-loop contributions are given in Appendix B 3.

B.2 Form factors $H_{i,\tau}(s, t)$

The $H_{i,\tau}(s, t)$ are expressed by

$$\begin{aligned} H_{i,\tau}(s, t) = & \frac{\hat{e}^2}{s} \left\{ \left[Q_e \left(1 - \Pi_{T,\gamma}^{\gamma\gamma}(s) + \Gamma_1^e(s) \right) + T_e^3 \bar{\Gamma}_2^e(s) \right] h_i^{\gamma(0)} + Q_e h_i^{\gamma(1)}(s) \right\} \\ & + \frac{\hat{g}^2}{s - m_W^2/\hat{c}^2} \left\{ \left[(T_e^3 - \hat{s}^2 Q_e) \left(1 + \frac{\Delta}{s - m_W^2/\hat{c}^2} - \Pi_{T,Z}^{ZZ}(s) + \Gamma_1^e(s) \right) + T_e^3 (\hat{c}^2 \bar{\Gamma}_2^e(s) + \Gamma_3^e(s)) \right. \right. \\ & \left. \left. + \Gamma_4^e(s) \right] h_i^{Z(0)} + (T_e^3 - \hat{s}^2 Q_e) h_i^{Z(1)}(s) - \frac{\hat{s}}{\hat{c}} \left[(T_e^3 - \hat{s}^2 Q_e) h_i^{\gamma(0)} + Q_e \hat{c}^2 h_i^{Z(0)} \right] \Pi_{T,\gamma}^{Z\gamma}(s) \right\} \\ & + \frac{\hat{g}^2 T_e^3}{2t} \Gamma^{\nu\omega} + H_{i,\tau}^{[\text{Box}]}(s, t). \end{aligned} \quad (\text{B.4})$$

The vertex form factors are written as the sum of the tree-level and one-loop contributions by

$$h_i^V(s) = h_i^{V(0)} + h_i^{V(1)}(s), \quad (\text{B.5})$$

for $V = \gamma, Z$. The tree-level form-factor coefficients $h_i^{V(0)}$ are given by $h_i^{\gamma(0)} = \delta_{i1}$ and $h_i^{Z(0)} = -(\hat{s}^2/\hat{c}^2)\delta_{i1}$. The $h_i^{V(1)}(s)$ come from the one-loop 1PI $VW\chi$ vertex corrections. The chargino and neutralino contributions to $h_i^{V(1)}(s)$ are shown in Appendix B 5. All the one-loop vertex contributions $\Gamma_1^e, \bar{\Gamma}_2^e, \Gamma_3^e, \Gamma_4^e$, and $\Gamma^{\nu\omega}$ and the box diagrams $H_{i,\tau}^{[\text{Box}]}$ that connect with initial e^\pm lines turn out to be zero for the chargino and neutralino contributions.

B.3 Two-point functions

The explicit forms of the two-point functions of $\Pi_T^{\gamma\gamma}, \Pi_T^{\gamma Z}, \Pi_T^{ZZ}$, and Π_T^{WW} are the following [16].

$$\Pi_T^{\gamma\gamma} = \frac{\hat{e}^2}{16\pi^2} 8q^2 B_3(q^2, m_{\tilde{\chi}_i^-}, m_{\tilde{\chi}_i^-}), \quad (\text{B.6a})$$

$$\Pi_T^{\gamma Z} = \frac{\hat{e}\hat{g}_Z}{16\pi^2} \left\{ (D_L)_{ii} + (D_R)_{ii} - 2\hat{s}^2 \right\} 4q^2 B_3(q^2, m_{\tilde{\chi}_i^-}, m_{\tilde{\chi}_i^-}), \quad (\text{B.6b})$$

$$\begin{aligned}
\Pi_T^{ZZ} = & \frac{\hat{g}_Z^2}{16\pi^2} \left[\left\{ -\hat{s}^2 |(D_L)_{ii}|^2 - \hat{s}^2 |(D_R)_{ii}|^2 + \hat{s}^4 \right\} 8q^2 B_3(q^2, m_{\tilde{\chi}_i^-}, m_{\tilde{\chi}_i^-}) \right. \\
& 2 \left\{ |(D_L)_{ij}|^2 + |(D_R)_{ij}|^2 \right\} (2q^2 B_3 - B_4)(q^2, m_{\tilde{\chi}_i^-}, m_{\tilde{\chi}_j^-}) \\
& + 2m_{\tilde{\chi}_i^-} m_{\tilde{\chi}_j^-} \left\{ (D_L)_{ij} (D_R)_{ij}^* + (D_L)_{ij}^* (D_R)_{ij} \right\} B_0(q^2, m_{\tilde{\chi}_i^-}, m_{\tilde{\chi}_j^-}) \\
& + \left\{ |(N_L)_{ij}|^2 + |(N_R)_{ij}|^2 \right\} (2q^2 B_3 - B_4)(q^2, m_{\tilde{\chi}_i^0}, m_{\tilde{\chi}_j^0}) \\
& \left. + m_{\tilde{\chi}_i^0} m_{\tilde{\chi}_j^0} \left\{ (N_L)_{ij} (N_R)_{ij}^* + (N_L)_{ij}^* (N_R)_{ij} \right\} B_0(q^2, m_{\tilde{\chi}_i^0}, m_{\tilde{\chi}_j^0}) \right], \quad (B.6c)
\end{aligned}$$

$$\begin{aligned}
\Pi_T^{WW} = & \frac{\hat{g}^2}{16\pi^2} 2 \left[\left\{ |(C_L)_{ij}|^2 + |(C_R)_{ij}|^2 \right\} (2q^2 B_3 - B_4)(q^2, m_{\tilde{\chi}_i^0}, m_{\tilde{\chi}_j^0}) \right. \\
& \left. + m_{\tilde{\chi}_i^0} m_{\tilde{\chi}_j^0} \left\{ (C_L)_{ij} (C_R)_{ij}^* + (C_L)_{ij}^* (C_R)_{ij} \right\} B_0(q^2, m_{\tilde{\chi}_i^0}, m_{\tilde{\chi}_j^0}) \right], \quad (B.6d)
\end{aligned}$$

where

$$(C_\alpha)_{ij} = (U_\alpha^N)^*_{2i} (U_\alpha^C)_{1j} + \frac{1}{\sqrt{2}} (U_\alpha^N)^*_{3i} (U_\alpha^C)_{2j}, \quad (B.7a)$$

$$(D_\alpha)_{ij} = (U_\alpha^C)^*_{1i} (U_\alpha^C)_{1j} + \frac{1}{2} (U_\alpha^C)^*_{2i} (U_\alpha^C)_{2j}, \quad (B.7b)$$

$$(N_L)_{ij} = -(N_R)_{ij}^* = \frac{1}{2} \left\{ (U_L^N)^*_{3i} (U_L^N)_{3j} - (U_L^N)^*_{4i} (U_L^N)_{4j} \right\}. \quad (B.7c)$$

Here $\alpha = L$ or R in Eqs. (B.7a) and (B.7b).

The two-point functions Π_T^{QQ} , Π_T^{3Q} , Π_T^{33} , and Π_T^{11} can be written as $\Pi_T^{\gamma\gamma}$, $\Pi_T^{\gamma Z}$, Π_T^{ZZ} , and Π_T^{WW} . The relationships among them are shown in Eqs. (A1) of Ref. [11]. The gauge boson two-point functions $\Pi_{T,\gamma}^{\gamma\gamma}(q^2)$, $\Pi_{T,\gamma}^{\gamma Z}(q^2)$, and $\Pi_{T,Z}^{ZZ}(q^2)$ can be obtained from the transverse part of the vacuum polarization tensor

$$\Pi_{T,V_3}^{V_1 V_2}(q^2) = \frac{\Pi_T^{V_1 V_2}(q^2) - \Pi_T^{V_1 V_2}(m_{V_3}^2)}{q^2 - m_{V_3}^2}, \quad (B.8)$$

where V_1 , V_2 , and V_3 denote the gauge bosons. The one-loop chargino and neutralino contributions to the wave-function renormalization factor of the physical W boson are obtained from the WW two-point function Π_T^{WW}

$$Z_W^{\frac{1}{2}} = 1 - \frac{1}{2} \frac{d}{dq^2} \Pi_T^{WW}(q^2) \Big|_{q^2=m_W^2}, \quad \delta Z_W^{\frac{1}{2}} = Z_W^{\frac{1}{2}} - 1. \quad (B.9)$$

B.4 VW^+W^- triangle vertex functions

We discuss one-loop chargino and neutralino contributions to the VW^+W^- triangle vertex diagram [17]. The assignments of mass, momentum, and helicity of the couplings are shown in Fig. 10.

For evaluation of the loop integrals we use the convention of incoming momenta; hence we use $p_1 = -p$ and $p_2 = -\bar{p}$ where p and \bar{p} are defined in Fig. 10. Dropping the coupling factors, the tensor

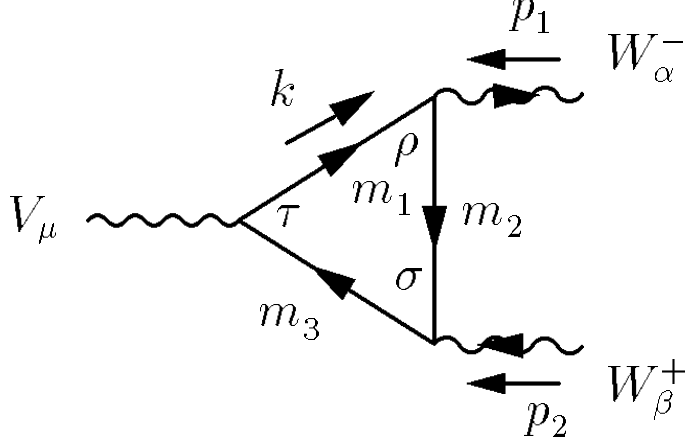


Figure 10: Mass and momentum assignments for the calculation of the chargino and neutralino triangle graph are shown. The arrows in the W lines indicate the flow of a negative electric charge.

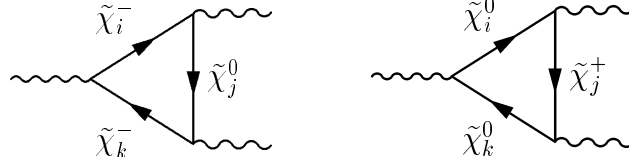


Figure 11: Feynman graphs contributing to the VW^+W^- vertex are shown. The mass and momentum assignments are shown in Fig. 10.

structure of the triangle diagram (Fig. 11) is given by

$$T_{\text{INOT}}^{\mu\alpha\beta}(p_1, p_2, m_1^2, m_2^2, m_3^2) = \sum_i C_i^{\text{INO}}(p_1, p_2, m_1^2, m_2^2, m_3^2) T_i^{\mu\alpha\beta} \quad (\text{B.10})$$

where the tensor structures of $T_i^{\mu\alpha\beta}$ are listed in Ref. [8]. The subscript “INOT” denotes “INO triangle” contributions. The nonzero C_i^{INO} are given by

$$\begin{aligned} C_1^{\text{INO}} = & \sum_{\tau=\sigma=\rho} m_W^2 \left(C_{31} - C_{32} - 3C_{33} + 3C_{34} - \frac{2-D}{m_W^2} C_{35} + \frac{2-D}{m_W^2} C_{36} + C_{21} + C_{22} - 2C_{23} \right. \\ & \left. + \frac{2-D}{m_W^2} C_{24} + \frac{s}{m_W^2} (C_{33} - C_{34} - C_{22} - C_{12}) \right) + \sum_{\tau=\sigma=-\rho} m_i m_j (-C_{11} + C_{12}) \\ & + \sum_{\tau=-\sigma=\rho} m_j m_k (-C_{11} + C_{12}) + \sum_{\tau=-\sigma=-\rho} m_k m_i (C_{11} - C_{12} + C_0), \end{aligned} \quad (\text{B.11a})$$

$$C_2^{\text{INO}} = \sum_{\tau=\sigma=\rho} m_W^2 (4C_{33} - 4C_{34} - 4C_{22} + 4C_{23}), \quad (\text{B.11b})$$

$$\begin{aligned} C_3^{\text{INO}} = & \sum_{\tau=\sigma=\rho} m_W^2 \left(-C_{31} + C_{32} + 3C_{33} - 3C_{34} + \frac{2-D}{m_W^2} C_{35} - \frac{2-D}{m_W^2} C_{36} \right. \\ & \left. - 3C_{21} - 3C_{22} + 6C_{23} + \frac{6-3D}{m_W^2} C_{24} - 2C_{11} + 2C_{12} \right) \end{aligned}$$

$$\begin{aligned}
& + \frac{s}{m_W^2}(-C_{33} + C_{34} + C_{22} - 2C_{23} - C_{12}) \Big) + \sum_{\tau=\sigma=-\rho} m_i m_j (C_{11} + C_{12} + 2C_0) \\
& + \sum_{\tau=-\sigma=\rho} m_j m_k (-C_{11} - C_{12}) + \sum_{\tau=-\sigma=-\rho} m_k m_i (C_{11} - C_{12} + C_0), \tag{B.11c}
\end{aligned}$$

$$\begin{aligned}
C_4^{\text{INO}} = & \sum_{\tau=\sigma=\rho} i m_W^2 \left(-C_{31} - C_{32} + C_{33} + C_{34} + \frac{2-D}{m_W^2} C_{35} + \frac{2-D}{m_W^2} C_{36} - C_{21} \right. \\
& \left. - C_{22} + 2C_{23} + \frac{2-D}{m_W^2} C_{24} + \frac{s}{m_W^2} (-C_{33} - C_{34} - C_{22} - 2C_{23} - C_{12}) \right) \\
& + \sum_{\tau=\sigma=-\rho} i m_i m_j (C_{11} - C_{12}) + \sum_{\tau=-\sigma=\rho} i m_j m_k (-C_{11} + C_{12}) \\
& + \sum_{\tau=-\sigma=-\rho} i m_k m_i (C_{11} + C_{12} + C_0), \tag{B.11d}
\end{aligned}$$

$$\begin{aligned}
C_5^{\text{INO}} = & \sum_{\tau=\sigma=\rho} \tau m_W^2 \left(C_{31} - C_{32} - 3C_{33} + 3C_{34} + \frac{2+D}{m_W^2} C_{35} - \frac{2+D}{m_W^2} C_{36} \right. \\
& \left. + C_{21} + C_{22} - 2C_{23} + \frac{2}{m_W^2} C_{24} + \frac{s}{m_W^2} (C_{33} - C_{34} - C_{22} + 2C_{23} + C_{12}) \right) \\
& + \sum_{\tau=\sigma=-\rho} \tau m_i m_j (-C_{11} + C_{12}) + \sum_{\tau=-\sigma=\rho} \tau m_j m_k (-C_{11} + C_{12}) \\
& + \sum_{\tau=-\sigma=-\rho} \tau m_k m_i (C_{11} - C_{12} + C_0), \tag{B.11e}
\end{aligned}$$

$$\begin{aligned}
C_6^{\text{INO}} = & \sum_{\tau=\sigma=\rho} -i \tau m_W^2 \left(C_{31} + C_{32} - C_{33} - C_{34} + \frac{2+D}{m_W^2} C_{35} + \frac{2+D}{m_W^2} C_{36} \right. \\
& \left. + 3C_{21} - C_{22} - 2C_{23} - \frac{2-2D}{m_W^2} C_{24} + 2C_{11} - 2C_{12} \right. \\
& \left. + \frac{s}{m_W^2} (C_{33} + C_{34} + C_{22} + 2C_{23} + C_{12}) \right) + \sum_{\tau=\sigma=-\rho} i \tau m_i m_j (C_{11} + C_{12} + 2C_0) \\
& + \sum_{\tau=-\sigma=\rho} i \tau m_j m_k (C_{11} + C_{12}) + \sum_{\tau=-\sigma=-\rho} i \tau m_k m_i (-C_{11} - C_{12} - C_0), \tag{B.11f}
\end{aligned}$$

$$\begin{aligned}
C_{10}^{\text{INO}} = & \sum_{\tau=\sigma=\rho} m_W^2 \left(2C_{31} - 2C_{32} - 6C_{33} + 6C_{34} - \frac{4-2D}{m_W^2} C_{35} + \frac{4-2D}{m_W^2} C_{36} \right. \\
& \left. + 2C_{21} + 2C_{22} - 4C_{23} - \frac{4-2D}{m_W^2} C_{24} \right. \\
& \left. + \frac{s}{m_W^2} (2C_{33} - 2C_{34} + 2C_{21} - 2C_{22} + 2C_{23} + 2C_{11}) \right) \\
& + \sum_{\tau=\sigma=-\rho} m_i m_j (2C_{11} - 2C_{12}) + \sum_{\tau=-\sigma=\rho} m_j m_k (-2C_{11} + 2C_{12}) \\
& + \sum_{\tau=-\sigma=-\rho} m_k m_i (-2C_{11} + 2C_{12} - 2C_0), \tag{B.11g}
\end{aligned}$$

$$C_{11}^{\text{INO}} = \sum_{\tau=\sigma=\rho} m_W^2 (-4C_{31} + 8C_{33} - 4C_{34} - 6C_{21} - 4C_{22} + 10C_{23} - 2C_{11} + 2C_{12}), \tag{B.11h}$$

$$C_{12}^{\text{INO}} = \sum_{\tau=\sigma=\rho} \tau m_W^2 (2C_{21} - 2C_{23} + 2C_{11} - 2C_{12}), \quad (\text{B.11i})$$

$$\begin{aligned} C_{13}^{\text{INO}} = & \sum_{\tau=\sigma=\rho} m_W^2 \left(-2C_{31} + 2C_{32} + 6C_{33} - 6C_{34} + \frac{4-2D}{m_W^2} C_{35} - \frac{4-2D}{m_W^2} C_{36} \right. \\ & \left. - 2C_{21} - 2C_{22} + 4C_{23} + \frac{4-2D}{m_W^2} C_{24} + \frac{s}{m_W^2} (-2C_{33} + 2C_{34} - 2C_{23} - 2C_{12}) \right) \\ & + \sum_{\tau=\sigma=-\rho} m_i m_j (2C_{11} - 2C_{12}) + \sum_{\tau=-\sigma=\rho} m_j m_k (-2C_{11} + 2C_{12}) \\ & + \sum_{\tau=-\sigma=-\rho} m_k m_i (2C_{11} - 2C_{12} + 2C_0), \end{aligned} \quad (\text{B.11j})$$

$$C_{14}^{\text{INO}} = \sum_{\tau=\sigma=\rho} m_W^2 (-4C_{32} - 4C_{33} + 8C_{34} + 2C_{22} - 2C_{23}), \quad (\text{B.11k})$$

$$C_{15}^{\text{INO}} = \sum_{\tau=\sigma=\rho} \tau m_W^2 (-2C_{22} + 2C_{23}), \quad (\text{B.11l})$$

$$C_{16}^{\text{INO}} = \sum_{\tau=\sigma=\rho} 4m_W^2 (-C_{31} + C_{32} + 3C_{33} - 3C_{34} - 2C_{21} - 2C_{22} + 4C_{23} - C_{11} + C_{12}). \quad (\text{B.11m})$$

The next step is to provide the correct couplings and masses and then sum over all triangle graphs. For the $\gamma W^+ W^-$ vertex,

$$f_i^{\gamma(1)\text{INOT}} = -\frac{1}{16\pi^2 \hat{e}} g_{\tau}^{\tilde{\chi}_i^- \tilde{\chi}_i^- A} g_{\sigma}^{\tilde{\chi}_i^- \tilde{\chi}_j^0 W} g_{\rho}^{\tilde{\chi}_j^0 \tilde{\chi}_i^- W} C_i^{\text{INO}}(p_1, p_2, m_{\tilde{\chi}_i^-}^2, m_{\tilde{\chi}_j^0}^2, m_{\tilde{\chi}_i^-}^2), \quad (\text{B.12})$$

where summation over charginos and neutralinos is implied. For the $ZW^+ W^-$ vertex,

$$\begin{aligned} f_i^{Z(1)\text{INOT}} = & -\frac{1}{16\pi^2 \hat{g}_Z \hat{e}^2} \left\{ g_{\tau}^{\tilde{\chi}_i^- \tilde{\chi}_k^- Z} g_{\sigma}^{\tilde{\chi}_k^0 \tilde{\chi}_j^0 W} g_{\rho}^{\tilde{\chi}_j^0 \tilde{\chi}_i^- W} C_i^{\text{INO}}(p_1, p_2, m_{\tilde{\chi}_i^-}^2, m_{\tilde{\chi}_j^0}^2, m_{\tilde{\chi}_k^-}^2) \right. \\ & \left. + g_{\tau}^{\tilde{\chi}_i^0 \tilde{\chi}_k^0 Z} g_{\sigma}^{\tilde{\chi}_k^0 \tilde{\chi}_j^+ W} g_{\rho}^{\tilde{\chi}_j^+ \tilde{\chi}_i^0 W} C_i^{\text{INO}}(p_1, p_2, m_{\tilde{\chi}_i^0}^2, m_{\tilde{\chi}_j^+}^2, m_{\tilde{\chi}_k^0}^2) \right\}, \end{aligned} \quad (\text{B.13})$$

where summation over charginos and neutralinos is implied.

B.5 $V\omega^+ W^-$ triangle vertex functions

We discuss one-loop chargino and neutralino contributions to the $V\omega^+ W^-$ triangle vertex diagram. The assignments of mass, momentum, and helicity of the couplings are in Fig. 12. Dropping the coupling factors, the tensor structure of the triangle diagram (Fig. 13) is given by

$$S_{\text{INOT}}^{\mu\alpha}(p_1, p_2, m_1^2, m_2^2, m_3^2) = \sum_i c_i^{\text{INO}}(p_1, p_2, m_1^2, m_2^2, m_3^2) S_i^{\mu\alpha}, \quad (\text{B.14})$$

where the tensor structures of $S_i^{\mu\alpha}$ are listed in Ref. [8]. The nonzero S_i^{INO} are given by

$$\begin{aligned} c_1^{\text{INO}} = & \sum_{\tau=-\sigma=-\rho} 2m_i m_W \left(C_{21} + C_{22} - 2C_{23} + \frac{D}{m_W^2} C_{24} + C_{11} - C_{12} + \frac{s}{m_W^2} (2C_{23} + C_{11} + 2C_{12} + C_0) \right) \\ & + \sum_{\tau=-\sigma=\rho} m_j m_W \left(-2C_{21} - 2C_{22} + 4C_{23} + \frac{4-2D}{m_W^2} C_{24} + \frac{s}{m_W^2} (-2C_{23} - C_{11} - C_{12}) \right) \end{aligned}$$

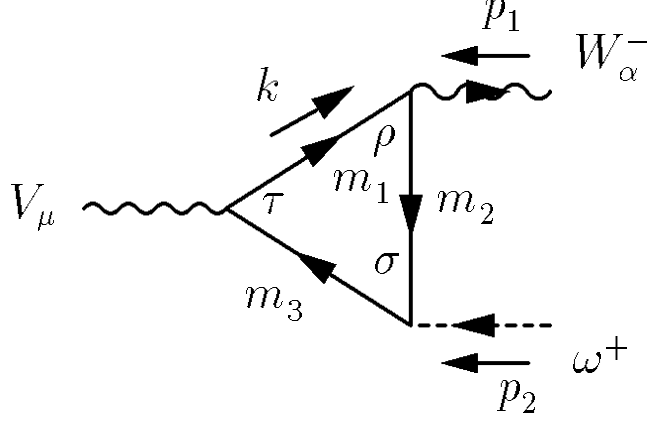


Figure 12: Mass and momentum assignments for the calculation of the chargino and neutralino triangle graph are shown. The arrows in the W lines indicate the flow of a negative electric charge.

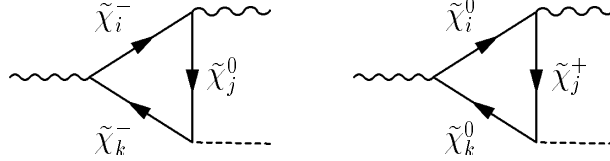


Figure 13: Feynman graphs contributing to the $V\omega^+W^-$ vertex are shown. The mass and momentum assignments are shown in Fig. 12.

$$\begin{aligned}
& + \sum_{\tau=\sigma=\rho} m_k m_W \left(-2C_{21} - 2C_{22} + 4C_{23} + \frac{4-2D}{m_W^2} C_{24} - 2C_{11} + 2C_{12} + \frac{s}{m_W^2} (-2C_{23} - C_{12}) \right) \\
& + \sum_{\tau=\sigma=-\rho} m_i m_j m_k \frac{1}{m_W} 2C_0, \tag{B.15a}
\end{aligned}$$

$$\begin{aligned}
c_2^{\text{INO}} &= \sum_{\tau=-\sigma=-\rho} m_i m_W (C_{11} + C_0) + \sum_{\tau=-\sigma=\rho} m_j m_W (2C_{22} - 2C_{23} - C_{11} + C_{12}) \\
& + \sum_{\tau=\sigma=\rho} m_k m_W (2C_{22} - 2C_{23} - C_{12}), \tag{B.15b}
\end{aligned}$$

$$c_3^{\text{INO}} = \sum_{\tau=-\sigma=-\rho} \tau m_i m_W (C_{11} + C_0) + \sum_{\tau=-\sigma=\rho} \tau m_j m_W (-C_{11} + C_{12}) + \sum_{\tau=\sigma=\rho} \tau m_k m_W (C_{12}), \tag{B.15c}$$

$$\begin{aligned}
c_4^{\text{INO}} &= \sum_{\tau=-\sigma=-\rho} m_i m_W (-2C_{11} - 2C_0) + \sum_{\tau=-\sigma=\rho} \tau m_j m_W (2C_{21} - 2C_{22} + 2C_{11} - 2C_{12}) \\
& + \sum_{\tau=\sigma=\rho} \tau m_k m_W (2C_{21} - 2C_{22} + 2C_{11}). \tag{B.15d}
\end{aligned}$$

The next step is to provide the correct couplings and masses and then sum over all triangle graphs. For the $\gamma\omega^+W^-$ vertex,

$$h_i^{\gamma(1)\text{INOT}} = -\frac{1}{16\pi^2 e} g_{\tau}^{\tilde{\chi}_i^- \tilde{\chi}_i^- A} g_{\sigma}^{\tilde{\chi}_i^- \tilde{\chi}_j^0 \omega} g_{\rho}^{\tilde{\chi}_j^0 \tilde{\chi}_i^- W} C_i^{\text{INO}}(p_1, p_2, m_{\tilde{\chi}_i^-}^2, m_{\tilde{\chi}_j^0}^2, m_{\tilde{\chi}_i^-}^2), \tag{B.16}$$

where summation over charginos and neutralinos is implied. For the $Z\omega^+W^-$ vertex,

$$h_i^{Z(1)\text{NOT}} = -\frac{1}{16\pi^2\hat{g}_Z\hat{c}^2} \left\{ g_\tau^{\tilde{\chi}_i^-\tilde{\chi}_k^-Z} g_\sigma^{\tilde{\chi}_k^-\tilde{\chi}_j^0\omega} g_\rho^{\tilde{\chi}_j^0\tilde{\chi}_i^-W} C_i^{\text{INO}}(p_1, p_2, m_{\tilde{\chi}_i^-}^2, m_{\tilde{\chi}_j^0}^2, m_{\tilde{\chi}_k^-}^2) \right. \\ \left. + g_\tau^{\tilde{\chi}_i^0\tilde{\chi}_k^0Z} g_\sigma^{\tilde{\chi}_k^0\tilde{\chi}_j^+\omega} g_\rho^{\tilde{\chi}_j^+\tilde{\chi}_i^0W} C_i^{\text{INO}}(p_1, p_2, m_{\tilde{\chi}_i^0}^2, m_{\tilde{\chi}_j^+}^2, m_{\tilde{\chi}_k^0}^2) \right\}. \quad (\text{B.17})$$

References

- [1] S. Alam, K. Hagiwara, S. Kanemura, R. Szalapski and Y. Umeda, Phys. Rev. **D62** (2000) 095011; K. Hagiwara, S. Kanemura and Y. Umeda, *Proceedings of 30th International Conference on High-Energy Physics (ICHEP 2000)*, [hep-ph/0009200].
- [2] T. Hahn, Nucl. Phys. **B 609** (2001) 344.
- [3] K.J.F. Gaemers and G.J. Gounaris, Z. Phys. **C1** (1979) 259.
- [4] K. Hagiwara, R.D. Peccei, D. Zeppenfeld and K. Hikasa, Nucl. Phys. **B282** (1987) 253.
- [5] J. Fleischer, F. Jegerlehner and M. Zralek, Z. Phys. **C42** (1989) 409; J. Fleischer, K. Kolodziej and F. Jegerlehner, Phys. Rev. **D47** (1993) 830.
- [6] K. Hagiwara, T. Hatsukano, S. Ishihara and R. Szalapski, Nucl. Phys. **B496** (1997) 66.
- [7] K. Hagiwara, S. Ishihara, R. Szalapski and D. Zeppenfeld, Phys. Rev. **D48** (1993) 2182.
- [8] S. Alam, K. Hagiwara, S. Kanemura, R. Szalapski and Y. Umeda, Nucl. Phys. **B541** (1999) 50.
- [9] O.V. Tarasov, A.A. Vladimirov and A.Yu. Zharkov, Phys. Lett. **93B** (1980) 429; K.G. Chetyrkin, A.L. Kataev and F.V. Tkachov, Nucl. Phys. **B174** (1980) 345.
- [10] G.C. Cho and K. Hagiwara, Nucl. Phys. **B 574** (2000) 623.
- [11] K. Hagiwara, D. Haidt, C. S. Kim and S. Matsumoto, Z. Phys. **C64** (1994) 559, Erratum, *ibid.* **C68** (1995) 352.
- [12] G.J. van Oldenborgh, Comput. Phys. Commun. **66** (1991) 1.
- [13] J. Ellis, S. Ferrara and D.V. Nanopoulos, Phys. Lett. **B114** (1982) 231; W. Buchmuller and D. Wyler, Phys. Lett. **B121** (1983) 321; J. Polchinski and M.B. Wise, Phys. Lett. **B125** (1983) 393.
- [14] T. Ibrahim and P. Nath, Phys. Lett. **B418** (1998) 98; T. Ibrahim and P. Nath, Phys. Rev. **D57** (1998) 478, Erratum *ibid.* **D58** (1998) 019901, Erratum-*ibid.* **D60** (1999) 079903, Erratum-*ibid.* **D60** (1999) 119901; T. Ibrahim and P. Nath, Phys. Rev. **D58** (1998) 111301; M. Brhlik, G.J. Good and G.L. Kane Phys. Rev. **D59** (1999) 115004.

- [15] M. Kitahara, M. Marui, N. Oshimo, T. Saito, and A. Sugamoto Eur. Phys. J. **C4** (1998) 661.
- [16] A. Dobado, M.J. Herrero and S. Penaranda Eur. Phys. J. **C7** (1999) 313.
- [17] A. Dobado, M.J. Herrero and S. Penaranda Eur. Phys. J. **C12** (2000) 637.